R. & M. No. 2946
(15,456)
A.R.C. Technical Report

MINISTRY OF SUPPLY

AERONAUTICAL RESEARCH COUNCIL
REPORTS AND MEMORANDA

Measurement of Lift, Pitching Moment and Hinge Moment on a Two-dimensional Cambered Aerofoil to Assist the Estimation of Camber Derivatives

By

H. C. GARNER, B.A., and A. S. BATSON, B.Sc.
of the Aerodynamics Division, N.P.L.

LONDON: HER MAJESTY'S STATIONERY OFFICE
1955
NINE SHILLINGS NET

Measurement of Lift, Pitching Moment and Hinge Moment on a Two-dimensional Cambered Aerofoil to Assist the Estimation of Camber Derivatives

By

H. C. GARNER, B.A., and A. S. BATSON, B.Sc.
of the Aerodynamics Division, N.P.L.

*Reports and Memoranda No. 2946**
December, 1952

Summary.—Aerodynamic camber derivatives are used in predicting three-dimensional control characteristics, in estimating wind-tunnel interference and in applying model data to full scale. Knowledge of these derivatives has been discussed in R. & M. 2820[1] (1950), from which it was apparent that experiments were needed to confirm empirical formulae for the derivatives of lift and pitching moment and to check widely differing formulae for the hinge-moment derivative.

A two-dimensional RAE 102 aerofoil with a 4 per cent parabolic centre-line and plain control surfaces of chord ratios 0·2 and 0·4 has been tested at a low speed and Reynolds number $0 \cdot 95 \times 10^6$. Particular attention is given to the effect of boundary-layer transition. Aerodynamic coefficients are obtained from measured forces and moments and from the pressure distribution at one section. The measured pressures compare fairly well with calculated distributions when the experimental circulation is used. Most of the coefficients from the integrated pressures are consistent with the balance measurements.

The empirical formulae for the camber derivatives of lift and pitching moment are consistent within about 6 per cent. A new formula for the hinge-moment derivative is suggested, which, though at times 25 per cent different from experiment, is believed to correspond to an aerodynamic camber as it normally operates on a lifting surface in incompressible viscous flow.

1. *Introduction.*—In assessing the present state of knowledge of aerodynamic camber derivatives, one of the authors[1] (1950) has suggested empirical formulae, but has shown the need for experiments to determine the hinge-moment derivative b' and to confirm the formulae for a' and m', the camber derivatives of lift and pitching moment. This supplementary information is necessary if two-dimensional data are to be used to predict three-dimensional control derivatives, especially $\partial C_H/\partial \alpha$, for which fairly accurate values of b' are required. Camber derivatives are also used in estimating tunnel interference and in applying model data to full scale.

In Ref. 1, four techniques for simulating aerodynamic camber have been discussed, namely :

(i) by using cambered models
(ii) by the principle of tunnel interference
(iii) by means of a whirling arm
(iv) by using a curved-flow tunnel.

The empirical formula for b' in Ref. 1 was based on the technique (ii). Hinge moments had been measured on given models under conditions such that the tunnel interference could be varied. However the estimated camber derivatives were not entirely consistent and only tentative conclusions were drawn.

* Published with the permission of the Director, National Physical Laboratory.

Technique (i) has been considered in this report, which describes tests on a two-dimensional cambered aerofoil, from which the derivatives a', m' and b' have been deduced. At the time of writing related tests are being carried out on the National Physical Laboratory Whirling Arm to provide comparisons by a third technique. These results will be reported separately.

2. NOTATION

a_1^*, m_1^*, b_1^*, a_2^*, etc.		Experimental derivatives, corrected for blockage only
a', m', b'		$\partial C_L/\partial\gamma$, $\partial C_m/\partial\gamma$, $\partial C_H/\partial\gamma$
a_1, m_1, b_1		$\partial C_L/\partial\alpha$, $\partial C_m/\partial\alpha$, $\partial C_H/\partial\alpha$
a_2, m_2, b_2		$\partial C_L/\partial\eta$, $\partial C_m/\partial\eta$, $\partial C_H/\partial\eta$
c		Chord of aerofoil (2·5 ft)
c_η		Chord of control, measured from hinge
C_L		$L/\frac{1}{2}\rho V^2 S$
C_m		$M/\frac{1}{2}\rho V^2 Sc$
C_H		$H/\frac{1}{2}\rho V^2 S_\eta c_\eta$
C_L^*, C_m^*, C_H^*		Coefficients corrected for blockage only
E	=	c_η/c
G	=	$\frac{1}{96}\pi(c/h)^2 = 0\cdot004175$
H		Hinge moment
h		Height of tunnel (7 ft)
J	=	$G(a_2^* + 4m_2^*)$
L		Lift
M		Pitching moment about quarter-chord
p		Pressure at surface of aerofoil
p_0		Pressure in undisturbed stream
R		Reynolds number ($0\cdot95 \times 10^6$)
S		Area of plan-form
S_η		Area of control
V		Wind speed
x, y		Ordinates of aerofoil referred to leading edge
x_t		Distance of transition from leading edge
α		Angle of incidence
α^*		Measured angle of incidence
γ		Camber $\left[\frac{\text{maximum ordinate of camber line}}{\text{chord of aerofoil}} = 0\cdot04\right]$
η		Control setting
λ		Nose balance as fraction of c_η
ρ		Density of air
τ		Trailing-edge angle (10° 55′)
Suffix $_u$		Denotes upper surface
,, $_l$		Denotes lower surface
,, $_T$		Denotes theoretical derivative
Prefix Δ		Denotes increment in allowing for tunnel interference
,, δ		Denotes increment due to change in transition.

3. *Description of Model.*—The model consisted of the aerofoil NPL 291 (Ref. 2) of basic fairing RAE 102 (Ref. 3) with a 4 per cent parabolic centre-line camber, which was mounted in the National Physical Laboratory 7-ft No. 3 Square Tunnel. The two-dimensional arrangement (Fig. 1) was substantially the same as that used for previous tests and shown in Figs. 3 and 4 of Ref. 4. The working portion of the aerofoil surface, finished in black french polish, was of 5-ft span, 30-in. chord and fitted with alternative plain controls, one of 6-in. chord, $E = 0 \cdot 2$, and the other of 1-ft chord, $E = 0 \cdot 4$. The model was constructed with special care and was accurate within 0·005 in. of the exact ordinates of the section, given in Table 1. A dummy end-piece of 1-ft span was fixed to each tunnel wall and could be aligned with the working portion to simulate two-dimensional conditions. There were clearance gaps of 0·3 in. between the working position and the dummies ; and pieces of fur-fabric were inserted to prevent the flow of air through them.

To prevent distortion under load, which had occurred with a previous model, the aerofoil and control were stiffened with steel bars and the spindles supporting the model were of increased diameter 1·125 in. These spindles, to which ball-races were attached, located the pitching axis at the quarter-chord position. This position had the advantage that the variation of pitching moment with angle of incidence was small. Since the aerofoil was tail heavy about the pitching axis, counterbalance weights were hung from the leading edge. The necessary leverage for the pitching-moment wire was obtained by means of a sting fastened to the leading edge of the aerofoil.

For measuring pressure distributions, copper tubes, of 0·094-in. outside diameter and 0·050-in. bore, were let into each surface along a section at 10 in. from the mid-span, where the flow was considered to be two-dimensional. Holes of 0·031-in. diameter were then drilled at the positions where pressures were to be measured. In order to facilitate the drilling and to give the aerofoil as smooth a surface as possible, the tubes, before insertion, were slightly flattened by running them through rollers. Each copper tube was connected to a manometer, on which the pressures were measured against the undisturbed static pressure. In this way, observations could be taken simultaneously.

4. *Scope and Accuracy of Tests.*—The scope of the experiments is given fully in Table 2. Lift, pitching moment and hinge moment were measured on roof balances ; and isolated pressures along both surfaces of one section were measured on a multi-tube manometer.

In carrying out these experiments, great care was required in setting the incidence of the main aerofoil and control surfaces to a horizontal datum position. Balance readings were taken with the model both ways up, *i.e.*, with positive and negative camber. Subsequent repeated readings established that the incidence was accurate within about 2 minutes.

There is evidence that the direction of flow in the tunnel may have changed during the course of the experiments. At the end of section 7 it has been deduced that a change of about 5 minutes occurred. This would amount to a change of about 0·008 in C_L, but would not affect the experimental slope of the lift curve. Since the results of the experiments for each control were consistent in themselves, the conditions in the tunnel room probably changed during the interval between the two experiments and affected the return flow of air.

It is believed that the results from both balance and pressure measurements were obtained with a fair degree of accuracy, the maximum departure from smooth curves being within 0·007 for C_L, 0·0010 for C_m, 0·0015 for C_H and 0·015 for $(p - p_0)/\frac{1}{2}\rho V^2$. As a check on accuracy, some incidences were repeated with the control rigidly fixed at neutral setting. The measured lift and pitching moment, plotted in Figs. 3 and 4, are seen to agree well within the stated accuracy.

The contribution to the hinge moment and pitching moment from the drag of the supporting wires was calculated and found to be negligible, the maximum recorded effect being of the order 0·0002 in C_H at $\alpha = 0$ deg, $\eta = +5$ deg. To ascertain the interference due to the sting forward of the leading edge, observations were taken with two additional dummy stings in position, The effect on lift and pitching moment was not measurable. After the experiments with the larger control were completed, it was found that the shroud just forward of the hinge had shrunk by about 0·015 in., but it seems unlikely that the small step caused by this shrinkage had any appreciable effect.

Apart from the effect of the small gap at the nose of the control on the natural transition, when $E = 0 \cdot 4$ (Fig. 2), the derivatives a_1, m_1, a' and m' should be the same for the two controls. The camber derivatives are in close agreement. However the two experimental values of a_1 differ by about 4·5 per cent on the smooth wing and 2·5 per cent when transition is fixed at 0·1 chord. There is at the same time a discrepancy of about 0·006-chord in aerodynamic centre, which rather exceeds the accountable error.

The most comprehensive check is the comparison of the coefficients C_L, C_m and C_H, as determined for a given setting of the model from balance measurements and integrated pressure distributions. The values of C_L with $E = 0 \cdot 4$, and C_m and C_H for both controls are satisfactorily within experimental error, as Tables 7, 8 and 9 show. When $E = 0 \cdot 2$, however, the integrated C_L is about 0·02 above the corresponding measured value, while the lift slopes are in fair agreement. This difference would be equivalent to a change in incidence of about 12·5 minutes. As a possible source of error a small spanwise variation of $\pm$ 2·5 minutes was detected from tip to tip, but the incidence, where the pressures were measured was a mean of the observations taken.

5. *Control of Transition*.—At the outset of the experiments wires of 0·022-in. diameter were used. Their effect was somewhat uncertain, as the diameter was smaller than the minimum diameter suggested in Ref. 5, section 3.1 and Fig. 1, namely :

at $x_t = 0 \cdot 1c$, not less than 0·020 in.
at $x_t = 0 \cdot 3c$, not less than 0·026 in.
at $x_t = 0 \cdot 5c$, not less than 0·029 in.

Therefore the diameter of the transition wires was increased to 0·028 in. at the position $x_t = 0 \cdot 3c$ and to $0 \cdot 032_5$ in. at $x_t = 0 \cdot 5c$.

With each control, $E = 0 \cdot 2$ and $E = 0 \cdot 4$, the points of natural transition were observed by the paraffin-evaporation method. The positions are shown plotted against angle of incidence in Figs. 2a and 2b, where the respective effects of camber and of E are given. Taking the case of positive camber, it is seen that transition on the upper surface remains back almost throughout the observed range of incidence, decreasing gradually from $x_t = 0 \cdot 73c$ at $\alpha = -6$ deg ($E = 0 \cdot 2$) to $x_t = 0 \cdot 55c$ at $\alpha = 3 \cdot 5$ deg ; however it rushes forward as α increases above 3·5 deg. At negative and small positive incidences a velocity peak near the leading edge of the lower surface (Fig. 12a) causes a forward transition, which travels backwards from $x_t = 0 \cdot 15c$ to $x_t = 0 \cdot 60c$ as α increases from -1 deg to $+2$ deg. It is thus seen that transition is back on both surfaces for the small range of incidence, approximately from $\alpha = 1$ deg to 3 deg. The agreement for positive camber and negative camber with sign of α changed is reasonably good.

Measurements of transition on a symmetrical RAE 102 aerofoil are included in Fig. 2a to compare curves of transition on the upper surface at positive, zero and negative camber.

In Fig. 2b, the observations for the two models show that the discontinuity in profile at the hinge has an effect on the transition where the natural position x_t exceeds $0 \cdot 6c$. This effect is most marked on the upper surface with negative camber and negative incidence. For most of the work at positive camber, when $0 \text{ deg} < \alpha < 4$ deg, this same effect was present on the lower surface, where transition never reached a position behind the hinge axis.

Transition was also observed at $\alpha = 0$ deg for a range of control setting $-5 \text{ deg} < \eta < +5$ deg ($E = 0 \cdot 4$) with positive camber. Most movement occurred on the lower surface from approximately $x_t = 0 \cdot 1c$ for $\eta = -5$ deg to $x_t = 0 \cdot 5c$ at $\eta = +5$ deg, as the forward suction peak disappeared. Transition was almost stationary at about $0 \cdot 65c$ on the upper surface, the total movement over the observed range of control setting being less than $0 \cdot 1c$.

6. *Balance Measurements*.—For $\eta = 0$ deg, the coefficients of lift, pitching moment and hinge moment, uncorrected for tunnel interference, are plotted against angle of incidence to the horizontal in Figs. 3, 4 and 5 for positive and negative camber when $E = 0 \cdot 2$, and for positive camber only when $E = 0 \cdot 4$. The signs of the coefficients and of incidence refer to the case of positive camber : and to illustrate the degree of scattering, observational points are given for one case only. When there is little or no change in transition with incidence, for example the smooth wing with 1 deg $< \alpha <$ 3 deg, it is seen that the observational points fall reasonably well on straight lines. Departure from linearity occurs around $\alpha = 4$ deg even with wires at $0 \cdot 1c$ and may indicate the beginning of a boundary layer separation on the upper surface. When the range of α for smooth wing in Fig. 3 is extended to $-$ 6 deg, it is found that no-lift occurs at approximately $\alpha = -4 \cdot 0$ deg with either flap at neutral setting.

The uncorrected coefficients C_L, C_m and C_H are also plotted against control setting in Figs. 6, 7 and 8. The aerofoil was set at positive camber with its chord-line approximately along the wind. For all cases of transition, the curves are straight over a range of control angle $-$ 5 deg $< \eta < +$ 2 deg. The departure from linearity at larger positive settings is most marked when transition is fixed at $x_t = 0 \cdot 1c$ and may again be due to the boundary layer on the upper surface.

Some experiments ($\eta = 0$ deg) were carried out with a wire on one surface and natural transition on the other; the changes in the uncorrected coefficients of lift, pitching moment and hinge moment with the position of wires are given in Figs. 9, 10 and 11. Four cases have been considered, namely :

(i) wire on lower surface, negative camber, $E = 0 \cdot 2$

(ii) wire on upper surface, positive camber, $E = 0 \cdot 2$

(iii) wire on upper surface, positive camber, $E = 0 \cdot 4$

(iv) wire on upper surface, negative camber, $E = 0 \cdot 4$.

The increment in each coefficient, as the transition is moved from $0 \cdot 1c$ to x_t, has been plotted against x_t/c and straight lines have been drawn allowing a reasonable scattering of the points. Figs. 9, 10 and 11 show that the slopes of the lines are independent of both E and sign of camber, and that there is a more marked effect, when transition is moved on the highly cambered surface. From such tests with the smaller control no consistent effect of incidence is apparent ; but with the larger control there is less scattering of points and the greater accuracy is sufficient to indicate a progressive increase in slope with increase in incidence, especially for lift and hinge moment. The tests with single wires on the flatter surface indicate that the effect of x_t is much smaller for all incidences. The change in the coefficients for a backward movement of transition, $\delta x_t = 0 \cdot 1c$ is given in the following table, the values being estimated for positive camber.

Model	Increment in coefficient	Upper surface (highly cambered surface)		Lower surface
		$\alpha = 0$ deg	$\alpha = 3$ deg	
$E = 0 \cdot 4$	δC_L	$+0 \cdot 005$	$+0 \cdot 007_5$	$-0 \cdot 000_5$
$E = 0 \cdot 4$	δC_m	$-0 \cdot 0011$	$-0 \cdot 0011$	$-0 \cdot 0004$
$E = 0 \cdot 4$	δC_H	$-0 \cdot 0021$	$-0 \cdot 0024$	$-0 \cdot 0005$
$E = 0 \cdot 2$	δC_H	$-0 \cdot 0020$	$-0 \cdot 0020$	—

7. *Tunnel Interference*.—The correction for tunnel blockage amounts to an increase of velocity

$$\frac{\Delta V}{V} = 0 \cdot 62 \frac{A'}{h^2} + \frac{C_D}{4} \cdot \frac{c}{h} = 0 \cdot 0059 \,, \qquad (1)$$

when $A' = \text{sectional area} = 0\cdot4076$ sq ft

$h = \text{height of tunnel} = 7$ ft

C_D is taken as $0\cdot008$.

The resulting increase in aerodynamic pressure ($\frac{1}{2}\rho V^2$) of $1\cdot2$ per cent gives a correction factor of $0\cdot988$. After applying this blockage correction, all the derivatives were corrected for tunnel interference as set out below.

From Ref. 5, equations (5) and (6),

$$\left.\begin{aligned}(\Delta\alpha) &= \frac{\pi}{96}\left(\frac{c}{h}\right)^2 (C_L^* + 4C_m^*)\\ (\Delta\gamma) &= \frac{\pi}{192}\left(\frac{c}{h}\right)^2 C_L^*\end{aligned}\right\} . \quad \ldots \quad (2)$$

$(\Delta\alpha)$ is applied as a correction to incidence, and

$(\Delta\gamma)$ is represented by corrections to the aerodynamic coefficients :

$$\left.\begin{aligned}(\Delta C_L) &= -a'(\Delta\gamma)\\ (\Delta C_M) &= -m'(\Delta\gamma)\\ (\Delta C_H) &= -b'(\Delta\gamma)\end{aligned}\right\} .$$

With the control at neutral setting the corrected derivatives are obtained as in the Appendix to Ref. 4 :

$$\left.\begin{aligned}a_1 &= \frac{C_L^* + (\Delta C_L)}{\alpha^* + (\Delta\alpha)} = \frac{a_1^* - \frac{1}{2}Ga_1^*a'}{1 + G(a_1^* + 4m_1^*)}\\ m_1 &= \frac{C_m^* + (\Delta C_m)}{\alpha^* + (\Delta\alpha)} = \frac{m_1^* - \frac{1}{2}Ga_1^*m'}{1 + G(a_1^* + 4m_1^*)}\\ b_1 &= \frac{C_H^* + (\Delta C_H)}{\alpha^* + (\Delta\alpha)} = \frac{b_1^* - \frac{1}{2}Ga_1^*b'}{1 + G(a_1^* + 4m_1^*)}\end{aligned}\right\} , \quad \ldots \quad (3)$$

where $G = \frac{\pi}{96}\left(\frac{c}{h}\right)^2 = 0\cdot004175,$

α^* is the measured incidence

a_1^*, m_1^*, b_1^* are the uncorrected derivatives

a', m', b' are taken from the experimental results, given in Tables 3 and 4.

From the measurements at zero α^*, the measured derivatives a_2^*, m_2^*, b_2^* with respect to control angle are corrected as in the Appendix to Ref. 4 :

$$\left.\begin{aligned}a_2 &= a_2^* - \tfrac{1}{2}Ga_2^*a' - Ja_1\\ m_2 &= m_2^* - \tfrac{1}{2}Ga_2^*m' - Jm_1\\ b_2 &= b_2^* - \tfrac{1}{2}Ga_2^*b' - Jb_1\end{aligned}\right\} , \quad \ldots \quad (4)$$

where $J = \frac{\Delta\alpha}{\eta} = G(a_2^* + 4m_2^*)$.

The measurements at $\alpha^* = 0$, $\eta = 0$ determine the camber derivatives ; and special care is needed in converting them to free-stream conditions. If α_1 and γ_1 represent the departure of tunnel flow from the horizontal, allowance for tunnel interference from (2) gives the result that the values, C_L^*, C_m^* and C_H^* correspond to an incidence and camber

$$\left.\begin{aligned} \alpha &= \alpha_1 + G(C_L^* + 4C_m^*) \\ \gamma &= \gamma_1 + \gamma_0 + \tfrac{1}{2}GC_L^* \end{aligned}\right\}, \qquad (5)$$

where $\gamma_0 = \pm 0\cdot04$ (centre-line camber of the aerofoil).

The experimental values of C_L^* and C_m^* are now substituted in the equation

$$\begin{aligned} C_L^* &= a_1\alpha + a'\gamma \\ &= a_1\{\alpha_1 + G(C_L^* + 4C_m^*)\} + a'(\gamma_1 + \gamma_0 + \tfrac{1}{2}GC_L^*), \end{aligned} \qquad (6)$$

where a_1 is given in equation (3). By taking differences between equations (6) for the positive and negative camber a' is given by

$$a'\left\{0\cdot08 + \tfrac{1}{2}G[C_L^*]^{\gamma_0 = +0\cdot04}_{\gamma_0 = -0\cdot04}\right\} = [C_L^* - a_1G(C_L^* + 4C_m^*)]^{\gamma = +0\cdot04}_{\gamma = -0\cdot04} \qquad (7)$$

Similarly m' and b' can be found from the equations :

$$\left.\begin{aligned} C_m^* &= m_1\{\alpha_1 + G(C_L^* + 4C_m^*)\} + m'(\gamma_1 + \gamma_0 + \tfrac{1}{2}GC_L^*) \\ C_H^* &= b_1\{\alpha_1 + G(C_L^* + 4C_m^*)\} + b'(\gamma_1 + \gamma_0 + \tfrac{1}{2}GC_L^*) \end{aligned}\right\}, \qquad (8)$$

where the first term involving m_1 or b_1 is small and can be neglected.

After the values of a', m' and b' have been obtained, the same pairs of equations may be added to give the values of α_1 and γ_1. These are given below for the smooth-wing case :

$$\left.\begin{aligned} \alpha_1 &= -0\cdot0021_5 \text{ radians} = -7 \text{ minutes } (E = 0\cdot2) \\ &= -0\cdot0005_7 \text{ radians} = -2 \text{ minutes } (E = 0\cdot4) \\ \gamma_1 &= +0\cdot0004_7 \quad = 0\cdot012\gamma_0 \quad (E = 0\cdot2) \\ &= +0\cdot0001_9 \quad = 0\cdot005\gamma_0 \quad (E = 0\cdot4) \end{aligned}\right\}.$$

These values, based on C_L^* and C_m^*, satisfy the equations based on C_H^* for the appropriate value of E, and, within experimental error, are independent of the position of transition wires. The different values of α_1 and γ_1 for the two models are attributed to changes of flow in the tunnel during the period that elapsed between the experiments on the $E = 0\cdot2$ and $E = 0\cdot4$ models.

8. *Camber Derivatives.*—The forces and moments on the cambered wing with zero incidence and control setting were determined from measurements when the chord-line of the aerofoil was horizontal, the experimental values being corrected both for blockage and tunnel interference, as shown in section 7. The derivatives a', b' and m' from balance measurements are given in Tables 3 and 4 together with theoretical values and those predicted from the formulae of Ref. 1. Variations with x_t/c, an equivalent position of transition, are shown in Figs. 15, 16 and 17 respectively, where values from integrated pressures are also included. In Fig. 2 it is seen that when $\alpha = 0$ deg the natural transition is asymmetrical, x_t being about $0\cdot3c$ on the lower surface and about $0\cdot65c$ on the upper surface. Hence, if wires are placed on both surfaces, where $x_t > 0\cdot3c$, transition will remain asymmetrical. For purposes of Figs. 15, 16 and 17, equivalent transitions for each aerodynamic coefficient have been estimated from section 6 as the symmetrical x_t that would keep the particular coefficient unaltered. This was done for the smooth wing case and for wires at $0\cdot5c$ and the resulting points were found to be well in line with the experimental ones for transition at $0\cdot1c$ and $0\cdot3c$.

Within the accuracy of the experiments the values of a' and m' are found to be independent of the model, apart from one case when a', calculated from pressure distribution ($E = 0\cdot2$), appears to be 5 to 6 per cent high. Otherwise, for each derivative, it has been possible to draw one line embracing all the observational points computed both from balance readings and from the integrated pressures.

The theoretical camber derivatives have been evaluated from thin-aerofoil theory,

$$\left.\begin{aligned} a'_T &= 4\pi \\ m'_T &= -\pi \\ b'_T &= -\frac{1}{E^2}[2(\pi - \theta_2)\cos\theta_1 + \sin 2\theta_2 \cos\theta_1 + \tfrac{4}{3}\sin^3\theta_2] \end{aligned}\right\}, \qquad (9)$$

where $\cos\theta_1 = 2E - 1$

and $\cos\theta_2 = 2(\lambda + 1)E - 1$,

λ being the chord of the nose balance as a fraction of the chord of the control. For a plain control without nose balance $\theta_1 = \theta_2$ and

$$b'_T = -\frac{1}{E^2}[2(\pi - \theta_1)\cos\theta_1 + \tfrac{3}{2}\sin\theta_1 + \tfrac{1}{6}\sin 3\theta_1].$$

To estimate the theoretical effect of the aerofoil shape, the pressure distribution from Goldstein's theory in Ref. 6 has been integrated (*see* section 10). The derivatives so obtained are compared with equation (9) in Tables 3 and 4.

Formulae for predicting the camber derivatives are taken from equations (6) and (7) of Ref. 1,

$$\frac{a'}{4\pi} = \frac{m'}{-\pi} = \frac{a_1}{(a_1)_T} \qquad (10)$$

and

$$b' = b_1\left(\frac{b'}{b_1}\right)_T, \qquad (11)$$

where $(a_1)_T$ is calculated in Ref. 7 (1951) and $(b'/b_1)_T$ is given in Table 2 of Ref. 5. Swanson and Crandall[8] (1947) have estimated that

$$\frac{b'}{b'_T} = 1 - 0\cdot0005\tau^2, \qquad (12)$$

where τ is the trailing-edge angle measured in degrees ($= 10\cdot91$ deg). The following new formula for b' is now suggested as being more consistent with equation (10) and rather closer to experiment than either (11) or (12) :

$$\frac{b'}{b'_T} = \frac{b_1}{(b_1)_T}, \qquad (13)$$

where b'_T is defined in equation (9), and unlike equation (11) $(b_1)_T$ includes the effect of wing thickness, so that $b_1/(b_1)_T$ may be estimated by the charts of Ref. 4.

This evaluation of b' together with the values of a' and m' from formula (10) has been plotted against x_t/c in Figs. 15, 16, 17. The experimental values of a' and $-m'$ are respectively smaller and larger than those estimated from (10). Figs. 15 and 16 show reductions of the order 7 per cent in a' and $5\cdot5$ per cent in $-m'$, as the transition moves forward from its natural position $x_t = 0\cdot64c$ to $x_t = 0\cdot1c$. Since the corresponding reduction in the experimental a_1 is only about 2 per cent, the formula (10) does not predict this. However the experiments confirm the formulae (10) within about 6 per cent. The experimental values of $-b'$ in Fig. 17 are considerably larger than those estimated from (13) with the corresponding experimental b_1 for the cambered model.

Fig. 18 shows theoretical curves of b' from thin- and thick-aerofoil theory plotted against E. Included in the same figure is the variation in b' from formula to formula ; and it is seen that (11) underestimates $-b'$ by rather less than (12) overestimates it, while (13), though close to (11), is in better agreement with experiment. The new formula still leaves discrepancies of the order 25 per cent in b', but it is thought that it should prove satisfactory in practical use.

The Reynolds number of test ($0 \cdot 95 \times 10^6$) is rather low and at a larger scale these discrepancies can be expected to decrease. The original formula (11) was based on the principle of tunnel interference (section 1) applied to three types of control surface of chord ratio $E = 0 \cdot 3$ (Kirk[9], 1943). There were indications that the formula was valid for overbalanced controls. The new formula (13), being similar, might be of more general application than one based solely on the present tests on plain controls.

The significant derivative b', required in the various calculations of $\partial C_H/\partial \alpha$ and tunnel interference, should correspond to the boundary layers present in the particular problem. Consider, for example, the derivative $\partial C_H/\partial \alpha$ for an uncambered swept wing. Apart from the non-linearity associated with viscous phenomena at moderate lift, the boundary layers have an effect similar to that on a two-dimensional uncambered wing (Ref. 10, Fig. 3, Küchemann, 1952).

Though a geometric and an aerodynamic camber are equivalent in potential flow, the loading due to an aerodynamic camber will usually operate under boundary-layer conditions different from those found on a two-dimensional cambered wing. The aerodynamic camber derivative of C_H and the geometric camber derivative from the present tests may differ somewhat. But the 4 per cent geometric camber is known to reduce $- b_1$ by about 10 per cent ; and it is recommended that the formula (13) should be used in conjunction with a b_1, measured or deduced from the charts of Ref. 4, for the particular basic section.

The following table gives the ratios $b_1/(b_1)_T$ for the aerofoil RAE 102 from experiment and from Figs. 29 and 30 of Ref. 4, associated with a mean lift slope $a_1 = 5 \cdot 5$, i.e., $a_1/(a_1)_T = 0 \cdot 81$, $\tau = 10 \cdot 9$ deg :

E	Condition	Cambered model	Uncambered model*	Ref. 4 $a_1 = 5 \cdot 5$
0·2	Smooth wing	0·40	0·49	0·69
0·2	0·1c wires	0·39	0·45	0·69
0·4	Smooth wing	0·61	0·67	0·71
0·4	0·1c wires	0·53	0·58	0·71

There are thus appreciable discrepancies between the charts of Ref. 4 and the experimental $b_1/(b_1)_T$ for the uncambered model. It is interesting to note that the average of these two ratios is close to the experimental b'/b'_T, when b'_T is taken from equation (9), *viz.*,

E	Condition	Average $\frac{b_1}{(b_1)_T}$	$\frac{b'}{b_T'}$
0·2	Smooth wing	0·59	0·62
0·2	0·1c wires	0·57	0·53
0·4	Smooth wing	0·69	0·71
0·4	0·1c wires	0·65	0·65

* These ratios $b_1/(b_1)_T$ are taken from data in C.P.191.

These comparisons suggest that the formula

$$\frac{b'}{b'_T} = \frac{b_1}{(b_1)_T} \quad \ldots \quad (13)$$

is as consistent as can reasonably be expected.

9. *Other Derivatives.*—The uncorrected derivatives with respect to incidence are given by the slopes of the straight lines in Figs. 3, 4 and 5, the limited range of incidence 1 deg $< \alpha <$ 3 deg being used when the transition is back. After applying a blockage correction from equation (1), the mean slopes for positive and negative camber have been corrected for tunnel interference by using equations (3) of section 7.

Similarly the uncorrected derivatives with respect to control setting for positive camber only are taken from the straight lines in Figs. 6, 7 and 8 for the limited range $-$ 5 deg $< \eta < +$ 2 deg. The mean slopes have been corrected by using equations (4) of section 7.

The values of a_1, m_1, b_1 and a_2, m_2, b_2, thus obtained, are given together with their theoretical values in Tables 3 and 4.

In general, with the exception of m_1, the experimental values become numerically smaller as transition is moved forward. m_1, which is small and positive, tends to become larger as x_t is reduced, so that the aerodynamic centre moves slightly forward. A comparison between the values of a_1 for the two models reveals that, as E is changed from $0 \cdot 2$ to $0 \cdot 4$, there is an increase of $4 \cdot 5$ per cent when the wing is smooth and $2 \cdot 5$ per cent when the transition is fixed at $x_t = 0 \cdot 1c$ on both surfaces. It is thought that similar tests on symmetrical models, now in progress, may explain this change in lift slope.

The experimental derivatives in Tables 3 and 4 have been compared with the charts of Ref. 4, when $\tau = 10 \cdot 9$ deg. Fair agreement in a_1 for the smooth wing is found (Ref. 4, Fig. 14), but the effect of movement of transition is less than the chart would suggest. When associated with the actual values of $a_1/(a_1)_T$ for the cambered wings, a_2 is reasonably consistent for $E = 0 \cdot 2$ and $E = 0 \cdot 4$ (Ref. 4, Fig. 18). In the case of derivatives b_1, b_2 for both controls and m_1, the experimental points, when plotted in Figs. 29, 30, 31, 32 and 65 of Ref. 4, fall on curves corresponding to a rather larger trailing-edge angle of about $\tau = 17$ deg. The derivative $m = - m_2 + m_1(a_2/a_1)$ in Ref. 4, Fig. 67, is found to be reasonably consistent for the smooth wing, while, as for a_1, the agreement is less good, when transition is forward.

10. *Theoretical Pressure Distributions.*—Although the empirical formulae, considered in section 8, involve only the theoretical camber derivatives for an aerofoil without thickness, it is desirable to investigate the effect of aerofoil fairing on these derivatives. Since a camber derivative strictly corresponds to the limiting condition $\gamma \to 0$, some calculations of chordwise loading were necessary to discover any non-linearity introduced by the camber of magnitude $\gamma = 0 \cdot 04$.

The pressure distributions have been calculated by Goldstein's Approximation III (Ref. 6) for the original unmodified RAE 102 with a 4 per cent parabolic camber-line, so that existing calculations for the symmetrical section by Pankhurst and Squire[3] (1950) could be used. The original rounded rear portion was flattened to a wedge from $0 \cdot 771c$ to the trailing edge in the actual fairing, defined in Ref. 3 and used in the present model (Table 1), but this modification should scarcely affect the pressures over most of the chord.

From equation (67) of Ref. 6, the non-dimensional velocity at the surface of the cambered aerofoil is

$$\frac{q}{V} = \frac{e^{C_0}(1 + \varepsilon')}{(\psi^2 + \sin^2 \theta)^{1/2}} \left| \left(1 - \frac{C_L^2}{a_1^2}\right)^{1/2} \sin(\theta + \varepsilon - \beta) + \frac{C_L}{a_1} \cos(\theta + \varepsilon - \beta) + \frac{C_L e^{-C_0}}{2\pi} \right|, \quad \ldots \quad (14)$$

where on the upper surface, $0 < \theta < \pi$,

$$\left.\begin{aligned} \psi_u &= \psi_s + 2\gamma \sin \theta \\ \varepsilon_u &= \varepsilon_s - 2\gamma \cos \theta \\ \varepsilon_u' &= \varepsilon_s' + 2\gamma \sin \theta \end{aligned}\right\},$$

on the lower surface, $-\pi < \theta < 0$,

$$\left.\begin{aligned} \psi_l &= \psi_s - 2\gamma \sin |\theta| \\ \varepsilon_l &= -\varepsilon_s - 2\gamma \cos \theta \\ \varepsilon_l' &= \varepsilon_s' - 2\gamma \sin |\theta| \end{aligned}\right\},$$

and

$$\left.\begin{aligned} \beta &= 2\gamma = 0\cdot08 \\ C_L &= a_1(\alpha + 2\gamma) \end{aligned}\right\}. \qquad (15)$$

The quantities

$$\psi_s(\theta) = 2y_s \operatorname{cosec} \theta$$

$$\varepsilon_s(\theta) = -\frac{1}{2\pi}\int_0^{\pi} \{\psi_s(\theta + t) - \psi_s(\theta - t)\} \cot \tfrac{1}{2}t\, dt$$

$$\varepsilon_s'(\theta) = d\varepsilon_s/d\theta$$

refer to the original symmetrical section, as calculated in Table 3 of Ref. 3. To the approximation of Ref. 6, θ is directly related to the chordwise distance

$$x = \tfrac{1}{2}c(1 - \cos \theta).$$

Then the pressure distribution

$$\frac{p - p_0}{\frac{1}{2}\rho V^2} = 1 - \left(\frac{q}{V}\right)^2 \qquad (16)$$

is calculated at once from equation (14). The lift in equation (15) is found to be about $\frac{1}{2}$ per cent greater than that obtained from the integral

$$C_L = \int_0^1 \frac{p_l - p_u}{\frac{1}{2}\rho V^2}\, d\left(\frac{x}{c}\right). \qquad (17)$$

The pitching moment is evaluated from the formula

$$-C_m = -\tfrac{1}{4}C_L + \int_0^1 \frac{p_l - p_0}{\frac{1}{2}\rho V^2}\left(\frac{x}{c} + \frac{y_l}{c}\frac{dy_l}{dx}\right) d\left(\frac{x}{c}\right) - \int_0^1 \frac{p_u - p_0}{\frac{1}{2}\rho V^2}\left(\frac{x}{c} + \frac{y_u}{c}\frac{dy_u}{dx}\right) d\left(\frac{x}{c}\right) \qquad (18)$$

where the ordinates y_l and y_u are given in Table 1. For moderate chord ratios the control hinge-moment coefficient is approximately

$$-C_H = \frac{\cos \frac{1}{2}\tau}{E}\int_{1-E}^1 \frac{p_l - p_u}{\frac{1}{2}\rho V^2}\left(\frac{x}{c} + E - 1\right) d\left(\frac{x}{c}\right), \qquad (19)$$

though the modification to sectional shape is probably appreciable.

Some of these formulae simplify when limiting camber is considered. As $\gamma \to 0$, equations (14) and (16) reduce to

$$\frac{p_l - p_u}{\frac{1}{2}\rho V^2} = \left(\frac{q}{V}\right)_0^2 . 8\gamma \left\{ \frac{\sin\theta}{1 + \varepsilon_s'} - \frac{\psi_s \sin\theta}{\psi_s^2 + \sin^2\theta} + \frac{1 - \cos\theta \cos(\theta + \varepsilon_s)}{\sin(\theta + \varepsilon_s)} \right\}, \quad .. \quad (20)$$

where $(q/V)_0$ corresponds to the symmetrical section at $C_L = 0$ and is given in Table 3 of Ref. 3. Values of $(p_l - p_u)/\frac{1}{2}\rho V^2\gamma$ from equation (20) are included in the final column of Table 2, and, in conjunction with formulae (17), (18) and (19), have been used to determine the theoretical derivatives

$$a' = \frac{\partial C_L}{\partial \gamma}, \; m' = \frac{\partial C_m}{\partial \gamma}, \; b' = \frac{\partial C_H}{\partial \gamma},$$

quoted in the columns, headed Ref. 6, in Tables 3 and 4. The effect of aerofoil shape is to increase a' and $-m'$ by 8 per cent and 4 per cent respectively and to decrease $-b'$ by 9 per cent, when $E = 0 \cdot 2$, and 4 per cent, when $E = 0 \cdot 4$. For each derivative the use of thick in place of thin aerofoil theory would not improve the empirical formulae, suggested in equations (10) and (13).

In equation (14), Joukowski's condition, $q/V = 0$ at the trailing edge, is satisfied if

$$a_1 = (a_1)_T = 2\pi \, e^{C_0} = 6 \cdot 79.$$

When this value is substituted in equation (15),

$$C_L = 0 \cdot 543, \text{ when } \alpha = 0.$$

The corresponding pressure distribution, plotted in Fig. 13, shows a slight peak suction forward at $0 \cdot 05c$ on the lower surface. A similar but more marked peak occurs experimentally. When the uncorrected experimental $C_L = 0 \cdot 422$ is substituted in equation (14) and

$$a_1 = \frac{0 \cdot 422}{0 \cdot 08} = 5 \cdot 28$$

is chosen to satisfy equation (15), the calculated peak suction on the lower surface is considerably enlarged and closely resembles the measured condition.

From equations (56) and (59) of Ref. 6, it will be seen that, since

$$\frac{dy_c}{dx} = 4\gamma \cos\theta,$$

$$\left.\begin{aligned} (C_L)_{\text{opt}}\left(\frac{1}{a_1} + \frac{1}{2\pi}\right) &= 4\gamma \\ \alpha_{\text{opt}}\left(\frac{1}{a_1} + \frac{1}{2\pi}\right) &= 2\gamma\left(\frac{1}{a_1} - \frac{1}{2\pi}\right) \end{aligned}\right\}.$$

Thus, on the basis of Goldstein's Approximation I, there is a stagnation point on the leading edge at the optimum incidence

$$\alpha_{\text{opt}} = \frac{0 \cdot 08 \, (2\pi - a_1)}{2\pi + a_1} \text{ radians},$$

which changes from $-0 \cdot 18$ deg to $+0 \cdot 30$ deg as the lift slope changes from its theoretical value $(a_1)_T = 6 \cdot 79$ to the mean experimental value $a_1 = 5 \cdot 50$. This indicates a tendency towards an unfavourable pressure gradient on the lower surface at $\alpha = 0$ as a_1 decreases. But, since the theoretical α_{opt} is negative, it is surprising to find even a small theoretical peak suction on the lower surface when $\alpha = 0$. This phenomenon may be peculiar to parabolic camber lines and partly due to the rather small C_L range of the basic RAE 102 section. It suggests, however, that some caution is necessary in estimating a practical α_{opt}.

The calculated pressure distributions, collected in Table 11, include two further examples :

$$\left.\begin{array}{l} \text{at } \alpha = -2 \text{ deg with experimental } C_L = 0{\cdot}215 \text{ and } a_1 = 4{\cdot}77 \\ \text{at } \alpha = +2 \text{ deg with experimental } C_L = 0{\cdot}638 \text{ and } a_1 = 5{\cdot}55 \end{array}\right\}.$$

In both cases the pressures over the forward part of the wing compare fairly well with experiment in Fig. 14. The coefficients C_L, C_m and C_H for $E = 0{\cdot}2$ and $0{\cdot}4$, integrated from equations (17), (18) and (19), are included at the foot of Table 11. The integrated C_L is about $0{\cdot}003$ low. Although C_m lies within 10 per cent of the uncorrected experimental value, the changes in C_m and more especially C_H are overestimated, when Joukowski's condition is relaxed to accommodate the experimental C_L. The hinge moments, so calculated, give small and uncertain values of $-b_1$.

From the theoretical pressures at $\alpha = 0$ deg with $a_1 = (a_1)_T$, the ratios

$$\frac{C_L}{0{\cdot}04}, \frac{C_m}{0{\cdot}04}, \frac{C_H}{0{\cdot}04}$$

calculated from equations (17), (18), (19), are found to lie well within $\frac{1}{2}$ per cent of the limiting derivatives as $\gamma \to 0$, deduced from equation (20). There is thus no theoretical reason for supposing that $\gamma = 0{\cdot}04$ is excessive for the purpose of obtaining camber derivatives. The calculated and uncorrected experimental coefficients for $\alpha = 0$, $\gamma = 0{\cdot}04$ are set out below :

Coefficient	(1) Thin-plate theory	(2) Ref. 6 $\gamma \to 0$	(3) Ref. 6 $C_L = 0{\cdot}543$	(4) Ref. 6 $C_L = 0{\cdot}422$	(5) Uncorrected experiment
C_L	0·502	0·542	0·540	0·419	0·422
C_m	−0·126	−0·130	−0·130	−0·106	−0·117
$C_H(E = 0{\cdot}2)$	−0·146	−0·132	−0·131	−0·069	−0·094
$C_H(E = 0{\cdot}4)$	−0·196	−0·188	−0·187	−0·124	−0·144

Columns (1) and (2) show the effect of aerofoil shape.

Columns (2) and (3) establish linearity with change in γ.

Columns (3) and (4) show the effect of changing the circulation to 0·78 of its theoretical value.

Columns (4) and (5) indicate the additional effect of viscosity in restoring finite conditions at the trailing edge.

11. *Measured Pressure Distributions.*—The results are presented as $(p - p_0)/\frac{1}{2}\rho V^2$ for each wing surface in Tables 5 and 6 in the respective cases $E = 0{\cdot}2$ and $E = 0{\cdot}4$. p_0, measured upstream of the working section, has not been corrected for pressure drop which is practically zero in the 7-ft wind tunnel.

For the first set of observations (at $\alpha = 0$ with $E = 0{\cdot}2$) the control was free with the usual small nose-gap, and the curve of $(p - p_0)/\frac{1}{2}\rho V^2$ against x/c showed a marked singularity at the hinge on the highly cambered upper surface. The control was afterwards rigidly fixed to the main aerofoil and the gap forward of the hinge filled in with wood extending 5 in. on each side of the section of pressure holes. It was hoped in this way to eliminate the singularity, which in fact was only slightly reduced; and the results showed that the pressure was sensitive to a discontinuity of surface, however small. All subsequent observations were taken with the control rigidly fixed.

The observational values of $(p - p_0)/\frac{1}{2}\rho V^2$ plotted against x/c showed a certain degree of scattering due mainly to the unsteadiness of the tunnel wind speed. As stated in section 4, the maximum departure from the smooth curve was of the order 0·015 in $(p - p_0)/\frac{1}{2}\rho V^2$. The curves without points are drawn for several incidences in Figs. 12a and 12b for $E = 0\cdot2$ and in Fig. 14 for $E = 0\cdot4$. Fig. 12a also shows the effect of transition on the pressure distribution at zero incidence. Fig. 14 includes a comparison between the experimental curves and those calculated for the same C_L. The calculations, described in section 10, were applied to an aerofoil of the given camber with the original unmodified fairing of RAE 102 with a rounded trailing edge, for which theoretical pressures were obtained in Ref. 3. Pressures for the cambered section at $\alpha = 0$, calculated from Ref. 6 for both the theoretical C_L of 0·543 and the measured C_L of 0·422, are plotted against x/c in Fig. 13 together with the experimental curves for both values of E. The agreement between experimental and calculated pressures is satisfactorily improved when the measured C_L is used.

For purposes of integration, the pressures near the hinge (*see* Fig. 12) and any transition wire were faired out. The integrated values of C_L, C_m and C_H together with those from balance measurements, all uncorrected for tunnel interference, are compared in Tables 7, 8 and 9.

In Table 7, the integrated values of C_L, when $E = 0\cdot2$, exceed the corresponding balance measurements by about 0·02. Though the integrations confirm the measured lift slope a_1, the camber derivative a' is dependent on the readings at $\alpha = 0$ and the estimate from pressure plotting is about 5 per cent high. These inconsistent values, shown in Fig. 15, do incidentally agree very closely with the estimate of a' from equation (10). A similar variation in hinge moment in Table 9 is barely significant. The integrated C_H is slightly more negative by roughly 0·0025.

When $E = 0\cdot4$, the comparisons of integrated and measured lift in Table 7 is shown to be within experimental error (section 4). The values of C_m in Table 8 are virtually independent of E and, like C_H in Table 9 for each control, the coefficients from the two sources agree well. The three camber derivatives m', b' $(E = 0\cdot2)$ and b' $(E = 0\cdot4)$, plotted against position of transition in Figs. 16 and 17, lie close to straight lines consistent with both pressure plotting and balance measurements.

12. *Concluding Remarks.*—The theoretical and measured experimental derivatives for the two-dimensional cambered RAE 102 section are summarized in Tables 3 and 4 for the two controls $E = 0\cdot2$ and $E = 0\cdot4$ respectively. The comparisons show greater changes in a_1, m_1 and b_1 with transition, when $E = 0\cdot4$; and for this control chord these derivatives and a_2, m_2 and b_2 are found to be closer to theory. There is a marked discrepancy of 4·5 per cent in a_1 with change of control chord. An identical discrepancy for a symmetrical RAE 102 aerofoil has since been measured and reported in C.P.191. Subsequent measurements for the same aerofoil without a control surface have shown that the true value of a_1 lies close to the value when $E = 0\cdot4$.

The effect of changing transition on one surface of the wing only is shown in Figs. 9, 10 and 11. As set out in section 6, there is little effect of incidence on the increments in aerodynamic coefficients with transition movement. Whilst C_L, C_m, and C_H are quite sensitive to the position of transition on the highly cambered surface, *viz.*,

$$\left.\begin{aligned} \delta C_L &= 0\cdot06\,\delta x_t/c \\ \delta C_m &= -0\cdot01\,\delta x_t/c \\ \delta C_H &= -0\cdot02\,\delta x_t/c \end{aligned}\right\} ,$$

the corresponding effect on the flatter surface is only one quarter as great.

From the measured pressures in Tables 5 and 6, the distributions are plotted for various incidences in Figs. 12 and 14. Calculated distributions compare fairly well, when the experimental C_L is used. At zero incidence there is a marked peak suction on the flatter surface which promotes a forward transition. In Fig. 13, it is interesting that this peak is rather less marked theoretically and becomes pronounced because only 0·8 of the theoretical lift is attained.

The coefficients obtained from integrated pressures are compared directly with the balance measurements in Tables 7, 8 and 9. Except for the coefficient C_L, when $E = 0{\cdot}2$, the results agree within the limits of experimental error. As described in section 4, special care was taken in setting the main aerofoil and control surfaces accurately within $\pm$ 2 minutes.

The chief purpose of the present investigation was to check existing empirical formulae for the camber derivatives of lift, pitching moment and hinge moment. Experimental values of a' and m', obtained from single observations at zero incidence, agree for the two controls within about 1 per cent and check the formulae within about 6 per cent (Figs. 15 and 16). Large differences between the formulae for b' and the experimental derivatives are shown in Fig. 18. For the reasons expressed in section 8, a new formula has been suggested. It is recommended that aerodynamic camber derivatives in incompressible viscous flow should be estimated as follows:

$$\frac{a'}{4\pi} = \frac{m'}{-\pi} = \frac{a_1}{(a_1)_T} \quad \ldots \quad (10)$$

$$\frac{b'}{b_T'} = \frac{b_1}{(b_1)_T} \quad \ldots \quad (13)$$

where $a_1/(a_1)_T$ and $b_1/(b_1)_T$ may be estimated from Ref. 4, and b_T' from thin aerofoil theory may be evaluated from Table 10.

Four techniques for simulating camber are discussed in Ref. 1:

(*a*) by using cambered models

(*b*) by the principle of tunnel interference

(*c*) by means of a whirling arm

(*d*) by using a curved-flow tunnel.

Technique (*a*) has led to the formulae (10). Both techniques (*a*) and (*b*) have been used in arriving at formula (13). Related tests are being carried out on the N.P.L. Whirling Arm and will be reported separately. The authors are unaware of any measurements of hinge moments in a curved-flow tunnel, and feel that such a check would be useful.

13. *Acknowledgments*.—The pressure-plotting and most of the balance measurements were carried by H. L. Nixon and W. C. Skelton. The authors also wish to acknowledge the assistance of Misses I. G. Davidson, E. Tingle, M. M. Stevens and S. E. Passmore with the experimental work.

REFERENCES

No.	Author	Title, etc.
1	H. C. Garner	Note on aerodynamic camber. R. & M. 2820. April, 1950.
2	R. C. Pankhurst	N.P.L. aerofoil catalogue and bibliography. C.P.81. July, 1951.
3	R. C. Pankhurst and H. B. Squire ..	Calculated pressure distributions for the RAE 100-104 aerofoil sections. C.P.80. March, 1950.
4	L. W. Bryant, A. S. Halliday and A. S. Batson.	Two-dimensional control characteristics. R. & M. 2730. April, 1950.
5	L. W. Bryant and H. C. Garner ..	Control testing in wind tunnels. R. & M. 2881. January, 1951.
6	S. Goldstein	Approximate two-dimensional aerofoil theory. Part II: Velocity distributions for cambered aerofoils. C.P.69. September, 1942.
7	H. C. Garner	Simple evaluation of the theoretical lift slope and aerodynamic centre of symmetrical aerofoils. R. & M. 2847. October, 1951.
8	R. S. Swanson and S. M. Crandall ..	Lifting-surface-theory aspect-ratio corrections to the lift and hinge-moment parameters for full-span elevators on horizontal tail surfaces. N.A.C.A. Tech. Note 1175. February, 1947.
9	F. N. Kirk	Wind-tunnel tests on tunnel corrections to hinge moments on control surfaces. R.A.E. Tech. Note Aero. 1277 (W.T.) A.R.C. 7148. 1943.
10	D. Küchemann	Some methods of determining the effect of the boundary layer on the lift slope of straight and swept wings. R.A.E. Tech. Note Aero. 2167. A.R.C. 15,245. June, 1952.

TABLE 1

Ordinates of Aerofoil Section (NPL 291)

Fairing : RAE 102
Maximum thickness $0 \cdot 10c$ at $0 \cdot 35c$

Camber : Parabolic camber-line.
Maximum camber $0 \cdot 04c$ at $0 \cdot 50c$

Leading-edge radius of curvature $= 0 \cdot 00686c$

Trailing-edge angle $= 10° 55'$

Aerofoil chord $= c$ $= 30$ in.

x/c (*from L.E.*)	*x* (*in.*)	*Upper surface* y_u (*in.*)	*Lower surface* y_l (*in.*)
0	0	0	0
0·005	0·150	0·2715	−0·2237
0·0075	0·225	0·3385	−0·2671
0·0125	0·375	0·4488	−0·3303
0·025	0·750	0·6632	−0·4292
0·05	1·500	0·9868	−0·5308
0·075	2·250	1·2454	−0·5794
0·10	3·000	1·4655	−0·6015
0·15	4·500	1·8272	−0·6032
0·20	6·000	2·1098	−0·5738
0·25	7·500	2·3278	−0·5278
0·30	9·000	2·4877	−0·4717
0·35	10·500	2·5918	−0·4078
0·40	12·000	2·6380	−0·3340
0·45	13·500	2·6190	−0·2430
0·50	15·000	2·5476	−0·1476
0·55	16·500	2·4320	−0·0560
0·60	18·000	2·2772	+0·0268
0·65	19·500	2·0874	0·0966
0·70	21·000	1·8659	0·1501
0·75	22·500	1·6162	0·1838
0·80	24·000	1·3411	0·1949
0·85	25·500	1·0418	0·1822
0·90	27·000	0·7185	0·1455
0·925	27·750	0·5479	0·1181
0·95	28·500	0·3713	0·0847
0·975	29·250	0·1886	0·0454
0·9875	29·625	0·0951	+0·0234
1	30·000	0	0

Note: y_u and y_l are measured in the same sense at right-angles to the chord line (joining the leading and trailing edges).

B

TABLE 2

Scope of Experiments

Balance Measurements of Lift, Pitching Moment and Hinge Moment

$\eta = 0$	Range of α to the horizontal (at intervals of 1 deg)			
	Model, $E = 0{\cdot}2$		Model, $E = 0{\cdot}4$	
	Positive camber	Negative camber	Positive camber	Negative camber
Smooth wing	−6, −4, −2 0 to 4	−4 to 0, 2, 4, 6, 8	−6, −4, −2 0 to 4	−4 to 0, 2, 4, 6
Wires at x_u and x_l $= 0{\cdot}1c$	−1 to +4	−4 to +1	−1 to +4	−4 to +1
$= 0{\cdot}3c$	0 to 4	−4 to 0	0 to 4	−4 to 0
$= 0{\cdot}5c$	0 to 4	−4 to 0	0 to 4	−4 to 0
Wires at x_u $= 0{\cdot}1c$	−1 to 4	—	0, 2, 4	−3, −2, 0
$= 0{\cdot}3c$	0 to 4	—	0, 2, 4	−3, −2, 0
$= 0{\cdot}5c$	0 to 4	—	0, 2, 3, 4	−3, −2, 0
Wires at x_l $= 0{\cdot}1c$	—	−4 to +1	—	—
$= 0{\cdot}3c$	—	−1, −3	—	—
$= 0{\cdot}5c$	—	−4 to 0	—	—
$\alpha = 0$	Control settings, $\eta = 0, \pm 1, \pm 3, \pm 5$ deg			
Smooth wing	−5 to +5	—	−5 to +5	—
Wires at x_u and x_l $= 0{\cdot}1c$	−5 to +5	—	−5 to +5	—
$= 0{\cdot}3c$	—	—	−5 to +5	—
$= 0{\cdot}5c$	−5 to +5	—	−5 to +5	—

Pressure Distributions

	α (deg) to the wind direction ($\eta = 0$)			
Smooth wing	−6, −4, −2, 0, +2	0	−2, 0, +2	—
Wires at x_u and x_l $= 0{\cdot}1c$	0	—	0	—
Wires at x_u and x_l $= 0{\cdot}3c$	—	—	0	—

$V = 60{\cdot}5$ ft/sec $\qquad R = 0{\cdot}95 \times 10^6$

TABLE 3

Calculated and Experimental Derivatives ($E = 0 \cdot 2$)

Derivative	Theoretical			Experimental			
	Thin aerofoil	Goldstein Ref. 6	Garner Ref. 7	Smooth wing	Wires at $0 \cdot 5c$	Wires at $0 \cdot 3c$	Wires at $0 \cdot 1c$
a_1	+6·283	+6·791	+6·767	+5·50	+5·46₅	+5·44	+5·43
m_1	0	−0·0720	−0·0704	+0·084	+0·080	+0·084	+0·086
b_1	−0·499	−0·431	—	−0·174	−0·184	−0·171	−0·169
a_2	+3·455	—	—	+2·59	+2·59	—	+2·41
m_2	−0·6400	—	—	−0·506	−0·499	—	−0·465
b_2	−0·923	—	—	−0·559	−0·554	—	−0·525
a'	+12·57	+13·55	—	+10·19	+10·05	+9·76	+9·40
Formula (10) (Ref. 1)	—	—	—	+10·18	+10·11	+10·06	+10·04
m'	−3·14	−3·26	—	−2·79	−2·77	−2·70	−2·64
Formula (10) (Ref. 1)	—	—	—	−2·55	−2·53	−2·52	−2·51
b'	−3·645	−3·30	—	−2·25	−2·17	−2·05	−1·95
Formula (11) (Ref. 1)	—	—	—	−1·27	−1·34	−1·25	−1·23
Formula (12) (Ref. 8)	—	—	—	−3·43	−3·43	−3·43	−3·43
New formula (13)	—	—	—	−1·47	−1·56	−1·45	−1·43

TABLE 4

Calculated and Experimental Derivatives ($E = 0 \cdot 4$)

Derivative	Theoretical			Experimental			
	Thin aerofoil	Goldstein Ref. 6	Garner Ref. 7	Smooth wing	Wires at $0 \cdot 5c$	Wires at $0 \cdot 3c$	Wires at $0 \cdot 1c$
a_1	+6·283	+6·791	+6·767	+5·75	+5·71	+5·62	+5·57
m_1	0	−0·0720	−0·0704	+0·041	+0·040	+0·048	+0·056
b_1	−0·745	−0·681	—	−0·414	−0·412	−0·387	−0·363
a_2	+4·698	—	—	+4·23	+4·14	+4·08	+4·00
m_2	−0·5879	—	—	−0·561	−0·548	−0·536	−0·526
b_2	−1·013	—	—	−0·754	−0·722	−0·701	−0·684
a'	+12·57	+13·55	—	+10·17	+9·94	+9·70	+9·50
Formula (10) (Ref. 1)	—	—	—	+10·68	+10·60	+10·44	+10·34
m'	−3·14	−3·26	—	−2·80	−2·73	−2·69	−2·64
Formula (10) (Ref. 1)	—	—	—	−2·67	−2·65	−2·61	−2·58
b'	−4·905	−4·70	—	−3·48	−3·37	−3·27	−3·19
Formula (11) (Ref. 1)	—	—	—	−2·73	−2·71	−2·55	−2·39
Formula (12) (Ref. 8)	—	—	—	−4·62	−4·62	−4·62	−4·62
New formula (13)	—	—	—	−2·98	−2·97	−2·79	−2·61

TABLE 5

Measured Pressure Distributions ($E = 0 \cdot 2, \eta = 0$)

Uncorrected Values of $\dfrac{p - p_0}{\frac{1}{2}\rho V^2}$

x/c	Upper surface						Lower surface
	Positive camber						Negative camber
	Smooth wing					Wires at 0·1c	Smooth wing
	$\alpha = -6°$	$-4°$	$-2°$	$0°$	$+2°$	$\alpha = 0°$	$\alpha = 0°$
0·0013	+0·435	+0·875	+0·982	+0·717	+0·049	+0·724	+0·725
0·0040	0·868	0·982	0·805	0·443	−0·203	0·446	0·401
0·0080	0·990	0·911	0·660	0·228	−0·408	0·277	+0·245
0·0160	0·911	0·727	0·436	+0·027	−0·520	+0·039	−0·034
0·0243	0·814	0·610	0·299	−0·062	−0·516	−0·029	−0·049
0·0370	0·675	0·461	0·184	−0·149	−0·471	−0·138	−0·134
0·0493	0·577	0·366	+0·102	−0·208	−0·567	−0·193	−0·189
0·0660	0·456	0·241	−0·011	−0·277	−0·589	−0·253	−0·273
0·0827	0·377	0·182	−0·049	−0·297	−0·584	−0·268	−0·286
0·0993	0·296	0·106	−0·104	−0·356	−0·608	—	−0·339
0·125	0·201	+0·015	−0·191	−0·406	−0·640	−0·350	−0·403
0·150	+0·100	−0·078	−0·286	−0·467	−0·687	−0·436	−0·452
0·199	−0·024	−0·186	−0·363	−0·536	−0·724	−0·509	−0·539
0·251	−0·131	−0·273	−0·434	−0·608	−0·757	−0·561	−0·597
0·299	−0·213	−0·346	−0·463	−0·624	−0·770	−0·609	−0·622
0·349	−0·268	−0·395	−0·510	−0·644	−0·767	−0·624	−0·640
0·399	−0·321	−0·432	−0·543	−0·655	−0·767	−0·640	−0·648
0·423	−0·339	−0·436	−0·555	−0·644	−0·766	−0·639	−0·652
0·449	−0·323	−0·436	−0·540	−0·638	−0·730	−0·604	−0·618
0·474	−0·338	−0·432	−0·528	−0·617	−0·717	−0·590	−0·612
0·499	−0·341	−0·430	−0·517	−0·602	−0·681	−0·569	−0·586

x/c	Lower surface						Upper surface
	Positive camber						Negative camber
	Smooth wing					Wires at 0·1c	Smooth wing
	$\alpha = -6°$	$-4°$	$-2°$	$0°$	$+2°$	$\alpha = 0°$	$\alpha = 0°$
0·0017	−3·725	−1·950	−0·412	+0·495	0·950	+0·455	+0·487
0·0043	−4·210	−2·466	−0·835	+0·164	0·696	+0·073	+0·115
0·0090	−3·340	−2·185	−1·030	−0·117	0·496	−0·182	−0·132
0·0170	−2·890	−1·765	−0·777	−0·188	0·285	−0·235	−0·189
0·0250	−1·842	−1·305	−0·745	−0·206	0·192	−0·317	−0·220
0·0380	−1·578	−1·042	−0·642	−0·228	0·131	−0·250	−0·245
0·0500	−1·292	−0·859	−0·553	−0·178	0·111	−0·195	−0·188
0·0670	−1·128	−0·745	−0·454	−0·168	0·073	−0·161	−0·165
0·0833	−0·929	−0·650	−0·387	−0·146	0·120	−0·140	−0·149
0·1003	−0·794	−0·561	−0·350	−0·131	0·084	—	−0·119
0·125	−0·693	−0·499	−0·305	−0·109	0·060	−0·075	−0·109
0·148	−0·619	−0·432	−0·250	−0·082	0·062	−0·080	−0·089
0·199	−0·487	−0·339	−0·191	−0·062	0·064	−0·062	−0·069
0·250	−0·407	−0·277	−0·148	−0·036	0·071	−0·051	−0·045
0·298	−0·328	−0·226	−0·118	−0·018	0·073	−0·025	−0·020
0·350	−0·276	−0·178	−0·086	+0·009	0·086	−0·011	+0·000
0·400	−0·222	−0·140	−0·062	0·020	0·088	+0·004	0·017
0·425	−0·186	−0·111	−0·040	0·031	0·100	0·026	0·024
0·450	−0·159	−0·089	−0·013	0·047	0·111	0·044	0·063
0·487	−0·124	−0·062	+0·009	0·068	0·126	0·062	0·073
0·498	−0·113	−0·042	+0·018	+0·075	0·128	+0·064	+0·079

TABLE 5—*continued*

Measured Pressure Distributions ($E = 0 \cdot 2, \eta = 0$)

Uncorrected values of $\dfrac{p - p_0}{\frac{1}{2}\rho V^2}$

x/c	Upper surface						Lower surface
	Positive camber						Negative camber
	Smooth wing					Wires at 0·1c	Smooth wing
	$\alpha = -6°$	$-4°$	$-2°$	$0°$	$+2°$	$\alpha = 0°$	$\alpha = 0°$
0·523	−0·339	−0·403	−0·502	−0·562	−0·675	−0·557	−0·561
0·539	−0·343	−0·399	−0·481	−0·540	−0·640	−0·531	−0·561
0·548	−0·325	−0·401	−0·487	−0·544	−0·631	−0·532	−0·550
0·598	−0·297	−0·357	−0·436	−0·480	−0·558	−0·472	−0·490
0·648	−0·248	−0·316	−0·383	−0·414	−0·460	−0·395	−0·414
0·698	−0·234	−0·271	−0·323	−0·365	−0·395	−0·350	−0·350
0·747	−0·197	−0·239	−0·265	−0·317	−0·341	−0·295	−0·297
0·786	−0·157	−0·180	−0·212	−0·253	−0·279	−0·237	−0·221
0·801	−0·179	−0·222	−0·250	−0·270	−0·290	−0·246	−0·268
0·816	−0·177	−0·202	−0·237	−0·246	−0·272	−0·228	−0·245
0·833	—	—	—	—	—	—	−0·224
0·850	−0·137	−0·153	−0·175	−0·182	−0·212	−0·175	−0·189
0·866	−0·120	−0·129	−0·142	−0·157	−0·182	−0·147	−0·168
0·883	−0·093	−0·110	−0·122	−0·124	−0·149$_5$	−0·124	−0·132
0·900	−0·064	−0·075	−0·086	−0·086	−0·110	−0·086	−0·094
0·917	−0·044	−0·053	−0·069	−0·062	−0·069	−0·066	−0·064
0·932	−0·022	−0·024	−0·031	−0·020	−0·047	−0·038	−0·026
0·950	+0·020	+0·000	+0·000	+0·009	+0·007	+0·005	+0·004
0·966	0·036	0·035	0·038	0·046	0·035	0·036	0·038
0·975	0·058	0·060	0·065	0·073	0·056	0·051	0·064
0·984	+0·082	+0·084	+0·089	+0·106	+0·076	+0·067	+0·092

x/c	Lower surface						Upper surface
	Positive camber						Negative camber
	Smooth wing					Wires at 0·1c	Smooth wing
	$\alpha = -6°$	$-4°$	$-2°$	$0°$	$+2°$	$\alpha = 0°$	$\alpha = 0°$
0·540	−0·077	−0·016	0·036	0·096	0·135	0·086	0·089
0·548	−0·071	−0·013	0·042	0·102	0·153	0·080	0·094
0·600	−0·022	+0·033	0·064	0·124	0·166	0·107	0·132
0·649	+0·020	0·055	0·098	0·138	0·182	0·131	0·134
0·698	0·042	0·078	0·120	0·157	0·186	0·146	0·162
0·737	0·062	0·098	0·142	0·171	0·200	0·159	0·165
0·781	0·077	0·109	0·140	0·173	0·195	0·153	0·168
0·801	0·091	0·117	0·149	0·173	0·199	0·158	0·175
0·816	0·091	0·117	0·139	0·173	0·195	0·153	0·188
0·833	0·091	0·117	0·148	0·177	0·191	0·161	0·188
0·849	0·099	0·126	0·142	0·177	0·193	0·164	0·181
0·867	0·104	0·131	0·152	0·173	0·197	0·158	0·188
0·883	0·106	0·135	0·157	0·173	0·195	0·158	0·189
0·900	0·118	0·140	0·162	0·178	0·199	0·161	0·189
0·916	0·120	0·144	0·157	0·178	0·195	0·155	0·186
0·933	0·120	0·142	0·157	0·173	0·191	0·146	0·188
0·950	0·133	0·148	0·159	0·173	0·186	0·144	0·189
0·966	0·131	0·146	0·157	0·171	0·168	0·135	0·171
0·975	0·135	0·148	0·157	0·162	0·155	0·135	0·164
0·983	0·140	0·149$_5$	0·166	0·157	0·177	0·133	0·166
0·986	+0·135	+0·144	0·159	0·155	0·151	0·126	0·158

TABLE 6

Measured Pressure Distributions ($E = 0 \cdot 4$, $\eta = 0$)

Uncorrected values of $(p - p_0)/\frac{1}{2}\rho V^2$

x_u/c	Upper surface, Positive camber, Smooth wing $\alpha = -2°$	Smooth wing $0°$	Smooth wing $+2°$	Wires at $0 \cdot 1c$ $\alpha = 0°$	Wires at $0 \cdot 3c$ $\alpha = 0°$	x_l/c	Lower surface, Positive camber, Smooth wing $\alpha = -2°$	Smooth wing $0°$	Smooth wing $+2°$	Wires at $0 \cdot 1c$ $\alpha = 0°$	Wires at $0 \cdot 3c$ $\alpha = 0°$
0·0013	+0·987	+0·765	+0·080	+0·805	+0·770	0·0017	−0·639	+0·463	0·930	+0·398	+0·407
0·0040	0·927	0·525	−0·192	0·544	0·553	0·0043	−0·941	+0·067	0·706	−0·027	+0·124
0·0080	0·705	0·264	−0·368	0·330	0·239	0·0090	−1·090	−0·215	0·452	−0·248	−0·249
0·0160	0·468	+0·056	−0·498	0·084	+0·061	0·0170	−0·891	−0·242	0·259	−0·288	−0·277
0·0243	0·257	−0·033	−0·500	+0·007	−0·004	0·0250	−0·806	−0·282	0·175	−0·315	−0·292
0·0370	0·214	−0·109	−0·524	−0·084	−0·097	0·0380	−0·695	−0·284	0·082	−0·310	−0·302
0·0493	0·126	−0·181	−0·556	−0·157	−0·162	0·0500	−0·610	−0·236	0·089	−0·257	−0·246
0·0660	+0·022	−0·269	−0·585	−0·232	−0·240	0·0670	−0·484	−0·199	0·073	−0·210	−0·219
0·0827	−0·022	−0·284	−0·571	−0·244	−0·262	0·0833	−0·407	−0·173	0·066	−0·178	−0·188
0·0993	−0·084	−0·321	−0·584	—	−0·312	0·1003	−0·341	−0·142	0·073	—	−0·160
0·125	−0·181	−0·398	−0·627	−0·315	−0·374	0·125	−0·318	−0·131	0·056	−0·118	−0·139
0·150	−0·248	−0·473	−0·671	−0·414	−0·432	0·148	−0·270	−0·108	0·062	−0·108	−0·118
0·199	−0·339	−0·539	−0·727	−0·492	−0·514	0·199	−0·210	−0·078	0·062	−0·084	−0·077
0·251	−0·412	−0·575	−0·757	−0·560	−0·550	0·250	−0·173	−0·060	0·060	−0·064	−0·051
0·299	−0·468	−0·614	−0·777	−0·596	—	0·298	−0·140	−0·021	$0 \cdot 067_5$	−0·042	—
0·349	−0·496	−0·623	−0·768	−0·607	−0·613	0·350	−0·106	+0·000	0·076	−0·026	−0·016
0·399	−0·530	−0·636	−0·762	−0·617	−0·620	0·400	−0·073	0·007	0·082	−0·011	+0·000
0·423	−0·525	−0·638	−0·768	−0·634	−0·612	0·425	−0·058	0·020	0·095	+0·011	0·011
0·449	−0·523	−0·612	−0·734	−0·600	−0·596	0·450	−0·035	0·047	0·106	0·040	0·038
0·474	−0·508	−0·596	−0·714	−0·575	−0·580	0·487	−0·013	0·056	0·120	0·033	0·047
0·499	−0·500	−0·596	−0·670	−0·558	−0·570	0·498	+0·005	0·056	0·135	0·058	0·062
0·523	−0·486	−0·554	−0·649	−0·538	−0·532	0·603	0·049	0·097	0·148	0·086	0·097
0·598	−0·432	−0·498	−0·549	−0·462	−0·460	0·651	0·086	0·135	0·165	0·120	0·117
0·643	−0·383	−0·434	−0·473	−0·408	−0·401	0·700	0·104	0·144	0·188	0·138	0·140
0·694	−0·330	−0·366	−0·425	−0·362	−0·367	0·738	0·129	0·164	0·198	0·148	0·151
0·733	−0·276	−0·326	−0·364	−0·314	−0·308	0·801	0·133	0·164	0·195	0·149	0·151
0·799	−0·219	−0·250	−0·275	−0·240	−0·244	0·817	0·139	0·164	0·196	0·148	0·153
0·814	−0·202	−0·239	−0·259	−0·213	−0·220	0·834	0·140	0·162	0·197	0·149	0·157
0·831	−0·195	−0·210	−0·249	−0·208	−0·212	0·851	0·146	0·162	0·195	0·151	0·157
0·849	−0·171	−0·200	−0·206	−0·177	−0·181	0·867	0·149	0·165	0·195	0·149	0·155
0·865	−0·140	−0·162	−0·179	−0·144	−0·148	0·885	0·149	0·164	0·186	0·149	0·155
0·882	−0·115	−0·129	−0·144	−0·115	−0·118	0·901	0·149	0·160	0·181	0·151	0·151
0·900	−0·091	−0·104	−0·115	−0·082	−0·080	0·918	0·148	0·164	0·181	0·138	0·148
0·916	−0·066	−0·066	−0·080	−0·055	−0·061	0·934	0·148	0·160	0·175	0·135	0·148
0·933	−0·031	−0·040	−0·047	−0·031	−0·031	0·952	0·148	0·160	0·168	0·137	0·138
0·950	−0·004	−0·007	−0·013	−0·002	+0·002	0·968	0·148	0·164	0·168	0·137	0·138
0·967	+0·035	+0·021	+0·027	+0·031	0·033	0·976	0·142	0·162	0·170	0·129	0·129
0·976	0·056	0·055	0·046	0·048	0·051	0·984	+0·144	+0·164	0·155	+0·128	+0·126
0·984	0·084	0·080	$0 \cdot 078_5$	0·067	0·067						
0·989	+0·093	+0·095	+0·084	+0·073	+0·075						

TABLE 7

Measured and Integrated Values of C_L

	α (deg)	C_L Integration	C_L Balance	C_L Balance, control rigidly fixed
		$E = 0 \cdot 2$, positive camber		
Smooth wing	+2	+0·648	+0·630	—
,,	0	0·442	0·422	—
,,	−2	0·237	0·207	—
,,	−4	+0·020	+0·006	—
,,	−6	−0·193	−0·200	—
Wires at 0·1c	0	+0·413	+0·381	—
		$E = 0 \cdot 2$, negative camber		
Smooth wing	0	−0·441	−0·421	—
		$E = 0 \cdot 4$, positive camber		
Smooth wing	+2	0·638	0·631	0·638
,,	0	0·422	0·419	0·414
,,	−2	0·215	0·208	—
Wires at 0·1c	0	0·384	0·394	0·391
Wires at 0·3c	0	0·394	0·401	—

TABLE 8

Measured and Integrated Values of C_m

	α (deg)	$-C_m$ Integration	$-C_m$ Balance	$-C_m$ Balance, control rigidly fixed
		$E = 0 \cdot 2$, positive camber		
Smooth wing	+2	0·117	$0 \cdot 115_5$	—
,,	0	$0 \cdot 114_5$	0·117	—
,,	−2	0·115	0·116	—
Wires at 0·1c	0	$0 \cdot 108_5$	0·109	—
		$E = 0 \cdot 4$, positive camber		
Smooth wing	+2	0·117	0·117	$0 \cdot 118_5$
,,	0	0·114	$0 \cdot 116_5$	0·118
,,	−2	0·108	$0 \cdot 115_5$	—
Wires at 0·1c	0	$0 \cdot 107_5$	$0 \cdot 110_5$	$0 \cdot 111_5$
Wires at 0·3c	0	0·109	0·112	—

TABLE 9

Measured and Integrated Values of C_H

	α (deg)	$-C_H$									
		$E = 0{\cdot}1$		0·2			0·3		0·4		
		Integrated		Balance	Integrated		Integrated		Integrated		Balance
		Model									
		20% flap	40% flap	20% flap		40% flap	20% flap	40% flap	20% flap	40% flap	
Smooth wing	−2	0·053	0·050	0·084$_5$	0·086	0·085$_5$	0·112	0·106$_5$	0·133	0·126	0·125$_5$
,,	0	0·055	0·059$_5$	0·093$_5$	0·095$_5$	0·099	0·123$_5$	0·123$_5$	0·147	0·147	0·144
,,	+2	0·067	0·067$_5$	0·101$_5$	0·108	0·112	0·140$_5$	0·140$_5$	0·168$_5$	0·168	0·162
Wires at 0·1c	0	0·047$_5$	0·048	0·080$_5$	0·083	0·084	0·111$_5$	0·109	0·135$_5$	0·133	0·132$_5$
Wires at 0·3c	0	—	0·050	—	—	0·089	—	0·114	—	0·137$_5$	0·135$_5$

TABLE 10

Values of $-b'$ from Thin Aerofoil Theory

λ	$(\lambda + 1)E$									
	0·08	0·10	0·15	0·20	0·25	0·30	0·35	0·40	0·45	0·50
0	2·372	2·640	3·196	3·648	4·029	4·360	4·649	4·905	5·132	5·333
0·05	2·306	2·567	3·110	3·552	3·927	4·252	4·537	4·791	5·018	5·220
0·10	2·222	2·475	3·001	3·430	3·795	4·112	4·393	4·644	4·869	5·071
0·15	2·121	2·363	2·868	3·281	3·634	3·942	4·216	4·462	4·684	4·886
0·20	2·002	2·232	2·712	3·106	3·444	3·741	4·007	4·246	4·464	4·664
0·25	1·866	2·081	2·532	2·904	3·225	3·509	3·764	3·996	4·209	4·406

TABLE 11

Calculated Pressure Distributions

x/c	Upper surface $\frac{p - p_0}{\frac{1}{2}\rho V^2}$				Lower surface $\frac{p - p_0}{\frac{1}{2}\rho V^2}$				$\frac{p_l - p_u}{\frac{1}{2}\rho V^2 \gamma}$
	$\alpha = 0°$ $C_L = 0·543$	$\alpha = -2°$ $C_L = 0·215$	$\alpha = 0°$ $C_L = 0·422$	$\alpha = +2°$ $C_L = 0·638$	$\alpha = 0°$ $C_L = 0·543$	$\alpha = -2°$ $C_L = 0·215$	$\alpha = 0°$ $C_L = 0·422$	$\alpha = +2°$ $C_L = 0·638$	$\gamma \to 0$
0	+1·0000	+0·3798	+0·9718	+0·7826	+1·0000	+0·3798	+0·9718	0·7826	0
0·001	0·7186	0·9787	0·8514	+0·1375	0·6941	−0·6016	0·5007	0·9821	−0·693
0·003	0·4195	0·9996	0·5881	−0·1910	0·3684	−0·9206	+0·1488	0·7998	−1·380
0·005	0·2550	0·8614	0·4256	−0·3257	0·2065	−0·9714	−0·0043	0·6523	−1·321
0·0075	+0·1272	0·7487	0·2922	−0·4117	+0·0957	−0·9555	−0·0991	0·5254	−0·890
0·0125	−0·0204	0·5791	+0·1307	−0·4918	−0·0083	−0·8771	−0·1758	0·3750	+0·216
0·025	−0·1896	0·3326	−0·0636	−0·5611	−0·0819	−0·7106	−0·2093	0·2165	2·643
0·05	−0·3303	+0·0946	−0·2295	−0·6090	−0·0919	−0·5236	−0·1843	0·1217	5·961
0·075	−0·4060	−0·0375	−0·3181	−0·6367	−0·0764	−0·4168	−0·1522	0·0933	8·272
0·10	−0·4590	−0·1285	−0·3792	−0·6585	−0·0586	−0·3441	−0·1243	0·0833	10·059
0·15	−0·5341	−0·2538	−0·4639	−0·6926	−0·0266	−0·2471	−0·0806	0·0806	12·750
0·20	−0·5873	−0·3405	−0·5227	−0·7180	−0·0010	−0·1833	−0·0484	0·0844	14·713
0·25	−0·6270	−0·4053	−0·5659	−0·7364	+0·0189	−0·1377	−0·0243	0·0888	16·204
0·30	−0·6570	−0·4554	−0·5983	−0·7486	0·0341	−0·1038	−0·0063	0·0922	17·322
0·35	−0·6792	−0·4945	−0·6219	−0·7552	0·0454	−0·0783	+0·0068	0·0937	18·152
0·40	−0·6945	−0·5244	−0·6381	−0·7564	0·0531	−0·0594	0·0156	0·0931	18·721
0·45	−0·6565	−0·5037	−0·6021	−0·7040	0·0881	−0·0121	0·0523	0·1196	18·643
0·50	−0·6137	−0·4759	−0·5607	−0·6481	0·1192	+0·0291	0·0847	0·1434	18·341
0·55	−0·5665	−0·4421	−0·5145	−0·5889	0·1466	0·0648	0·1128	0·1642	17·846
0·60	−0·5152	−0·4027	−0·4637	−0·5261	0·1705	0·0956	0·1369	0·1819	17·167
0·65	−0·4602	−0·3583	−0·4089	−0·4607	0·1910	0·1217	0·1571	0·1964	16·311
0·70	−0·4016	−0·3091	−0·3498	−0·3916	0·2079	0·1433	0·1733	0·2073	15·281
0·75	−0·3392	−0·2550	−0·2863	−0·3188	0·2212	0·1602	0·1851	0·2142	14·059
0·80	−0·2727	−0·1956	−0·2177	−0·2412	0·2302	0·1717	0·1915	0·2158	12·633
0·85	−0·2013	−0·1295	−0·1424	−0·1569	0·2340	0·1764	0·1908	0·2102	10·951
0·90	−0·1226	−0·0532	−0·0562	−0·0614	0·2304	0·1708	0·1786	0·1923	8·894
0·95	−0·0302	+0·0448	+0·0549	+0·0611	+0·2134	+0·1430	+0·1406	0·1457	+6·152
Integrated C_L					+0·540	+0·224	+0·419	+0·638	+13·55
Integrated C_m					−0·130	−0·196	−0·106	−0·103	−3·26
$C_H(E = 0·2)$					−0·131	−0·070	−0·069	−0·073	−3·30
$C_H(E = 0·4)$					−0·187	−0·121	−0·124	−0·144	−4·70

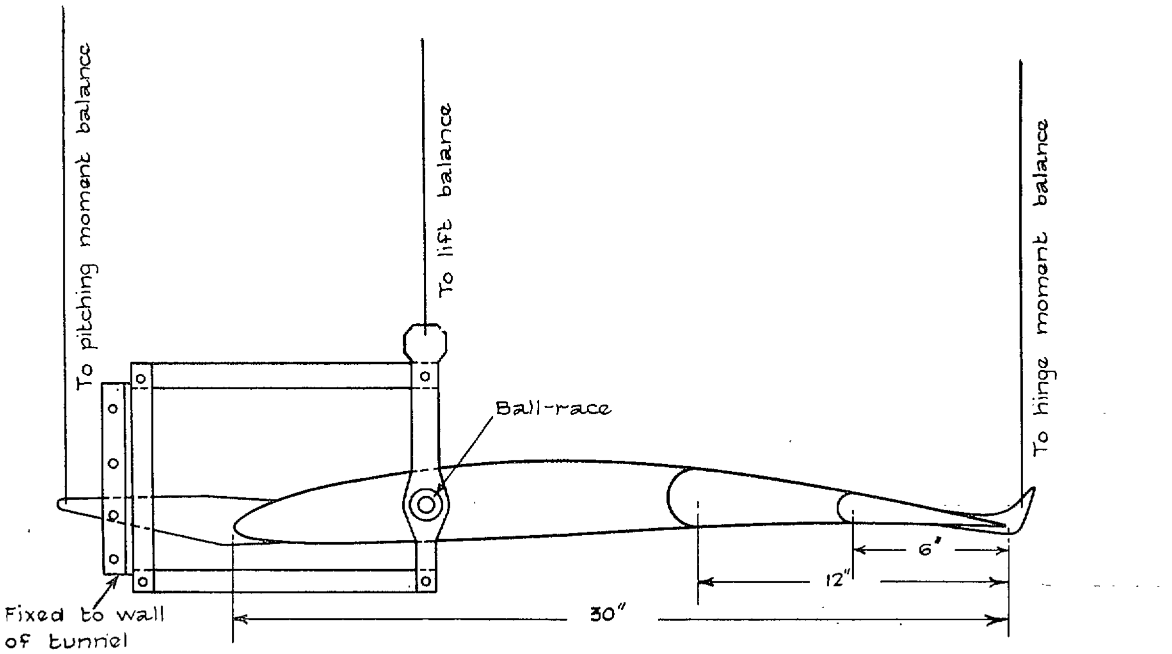

FIG. 1. Method of mounting the model.

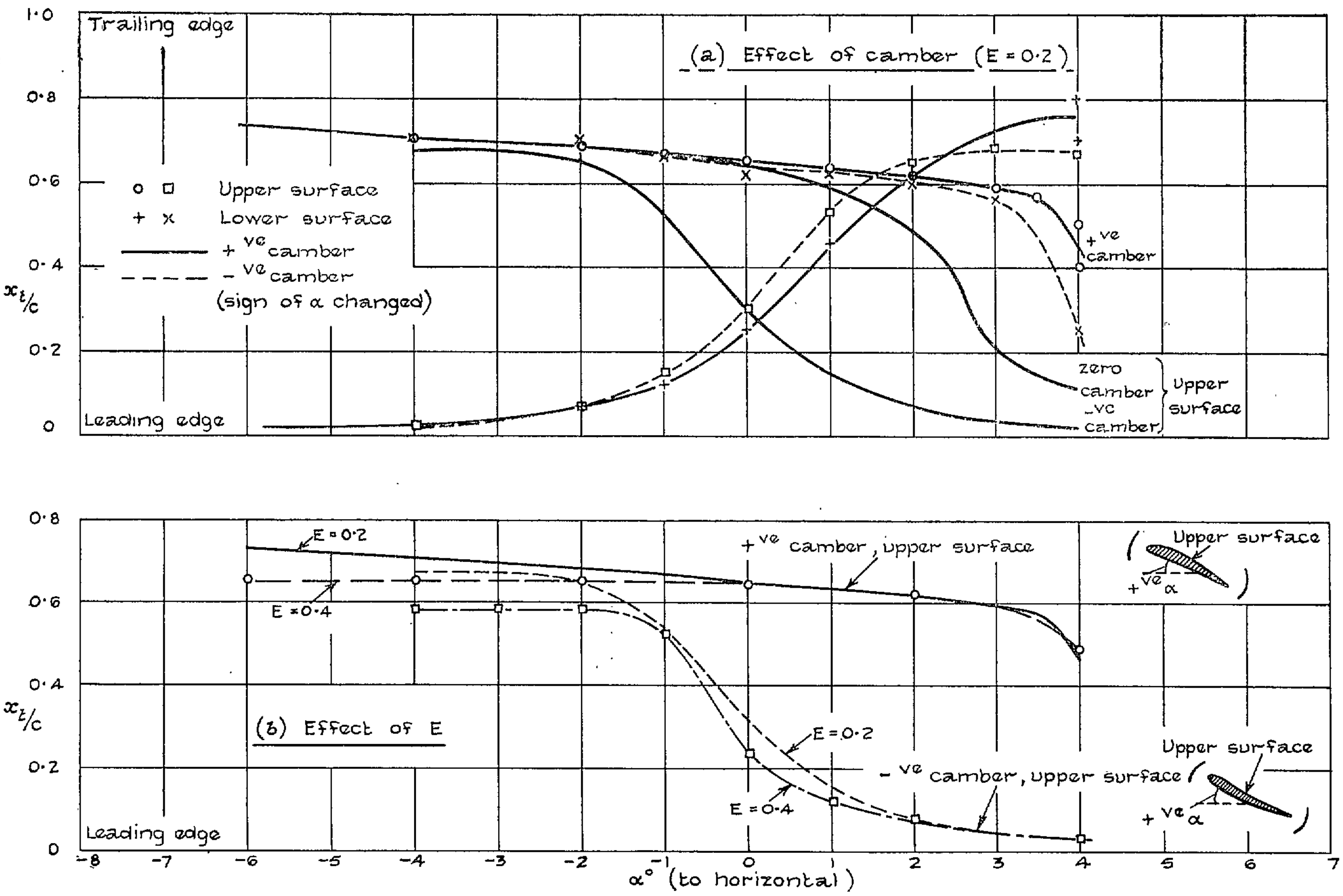

FIG. 2. Variation of natural transition with incidence.

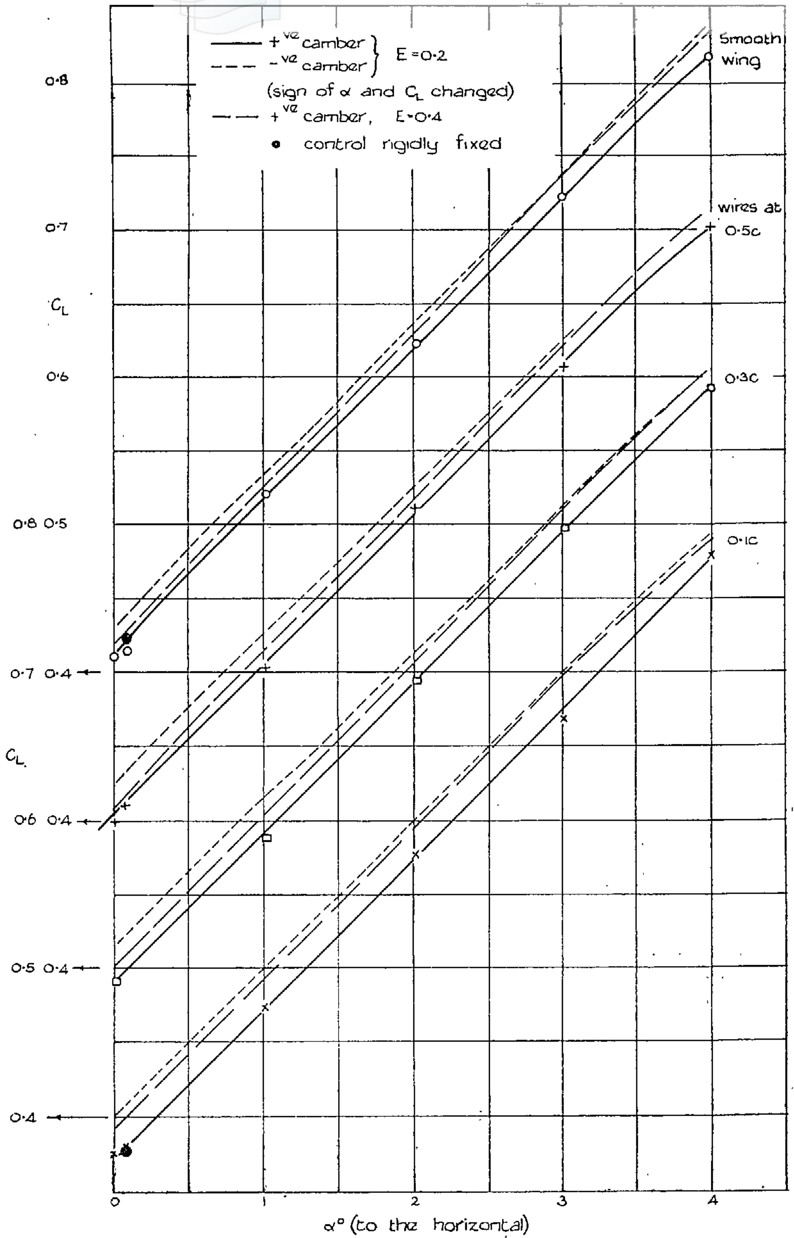

FIG. 3. Uncorrected lift against incidence.

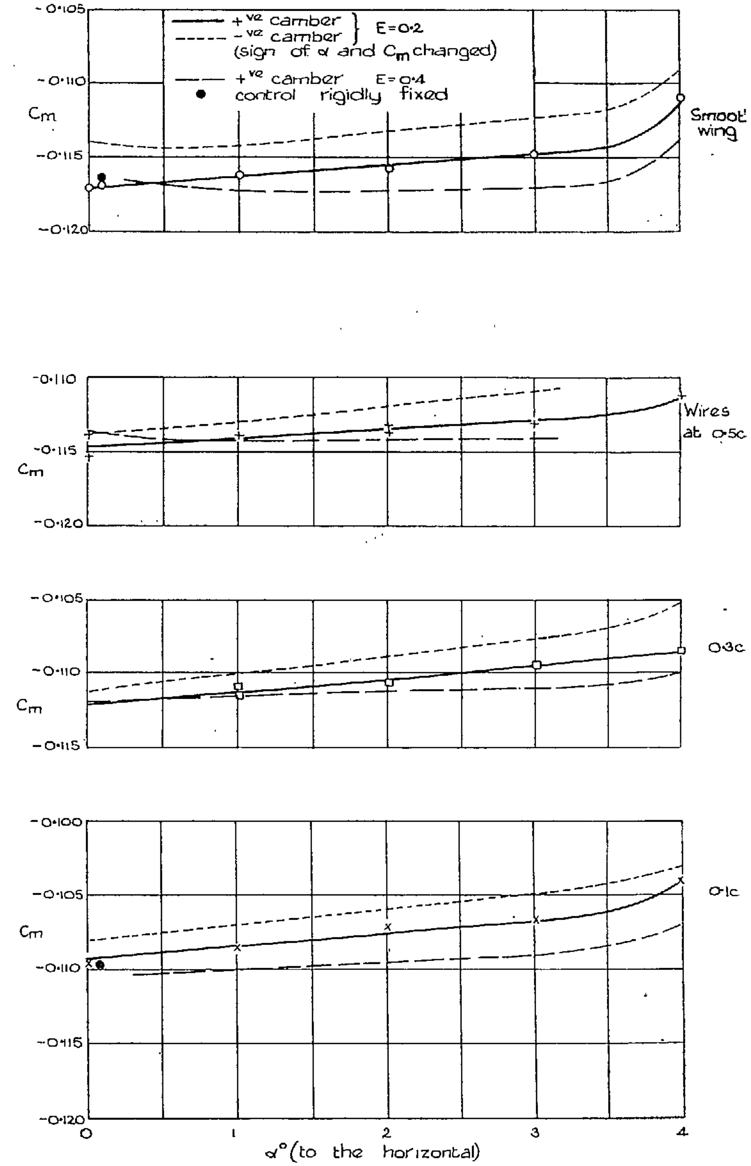

FIG. 4. Uncorrected pitching moment against incidence.

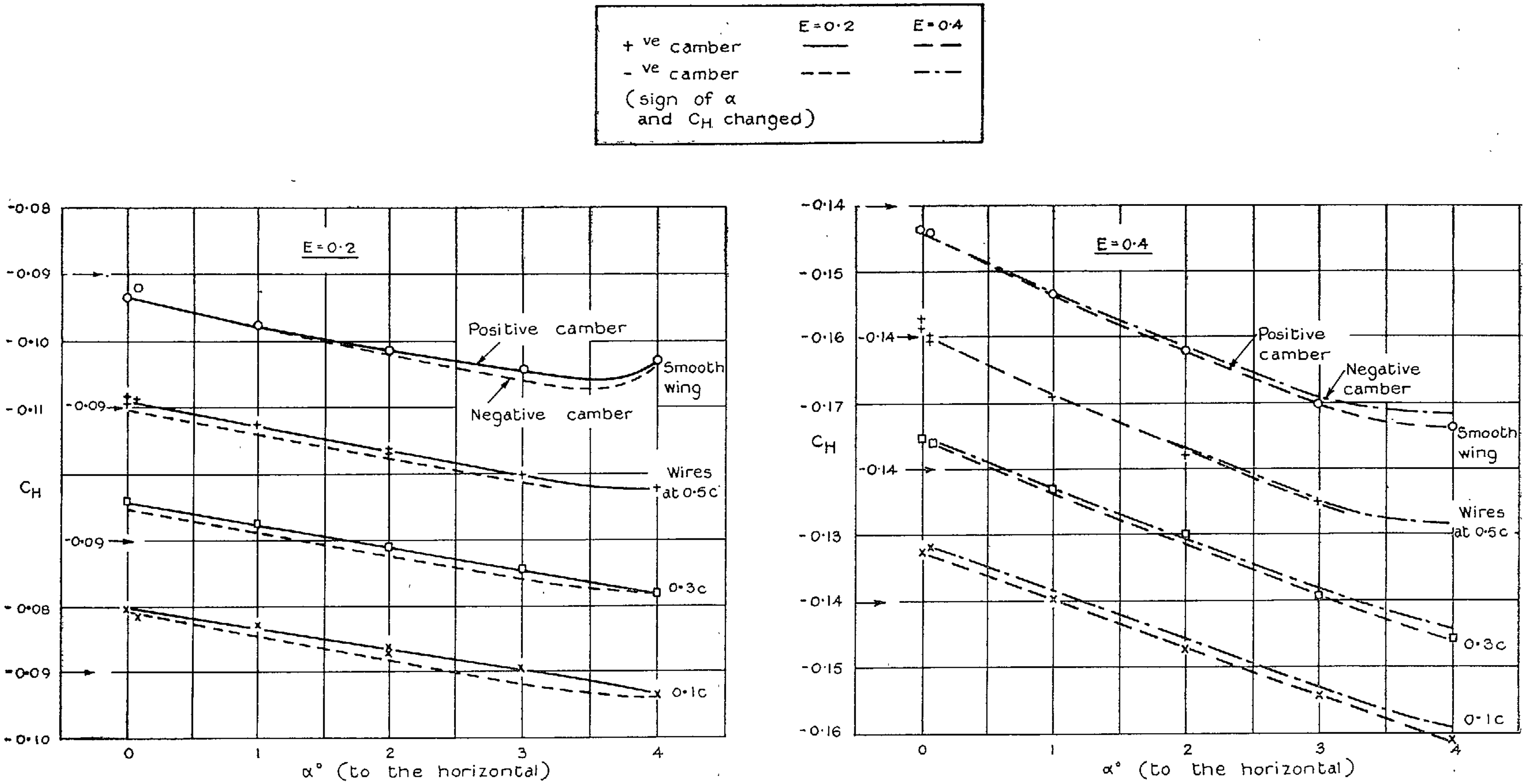

FIG. 5. Uncorrected hinge moment against incidence.

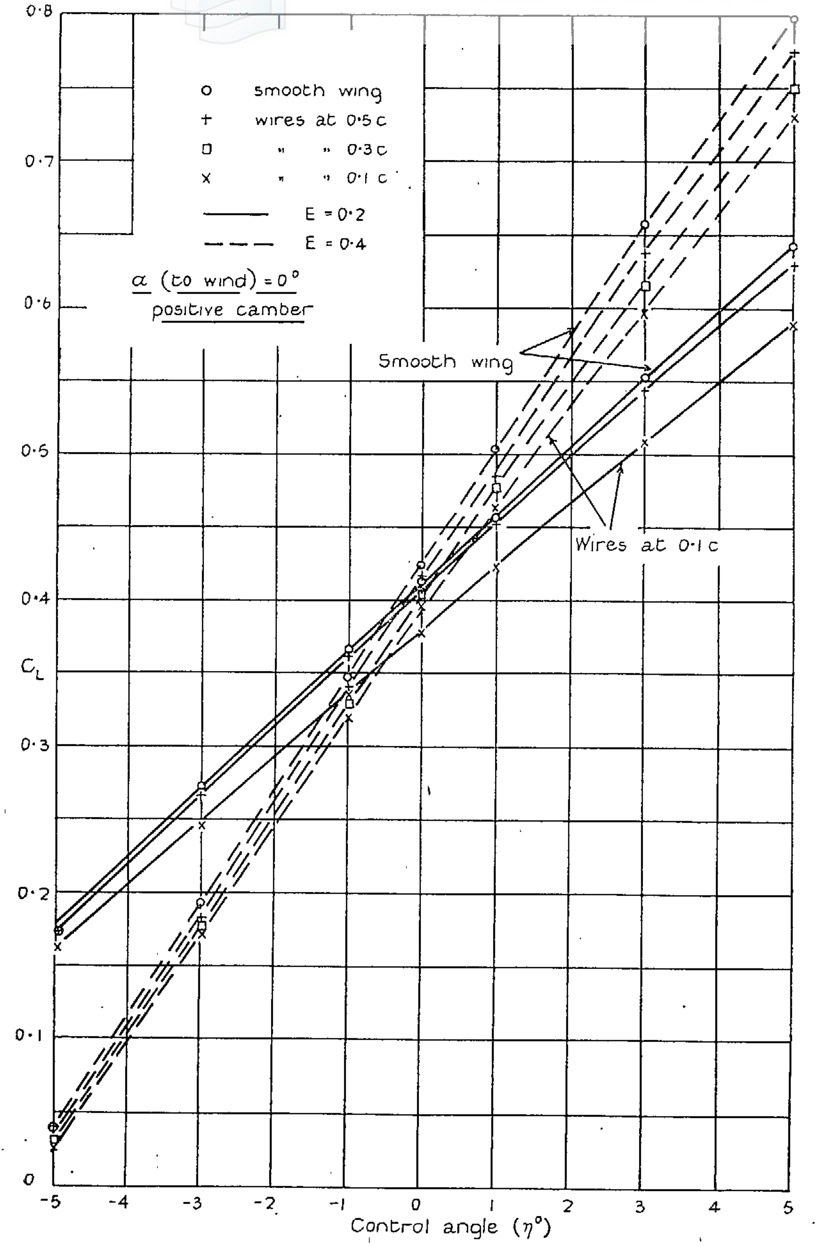

Fig. 6. Uncorrected lift against control setting.

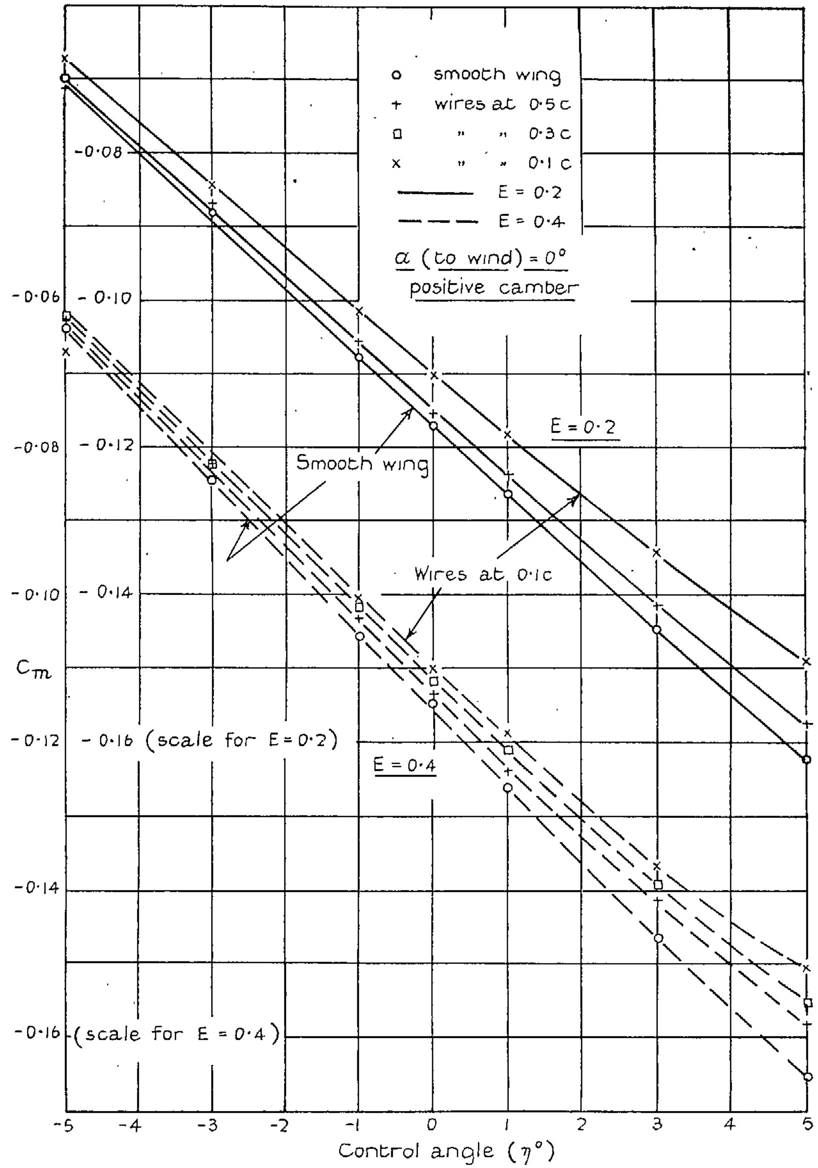

FIG. 7. Uncorrected pitching moment against control setting.

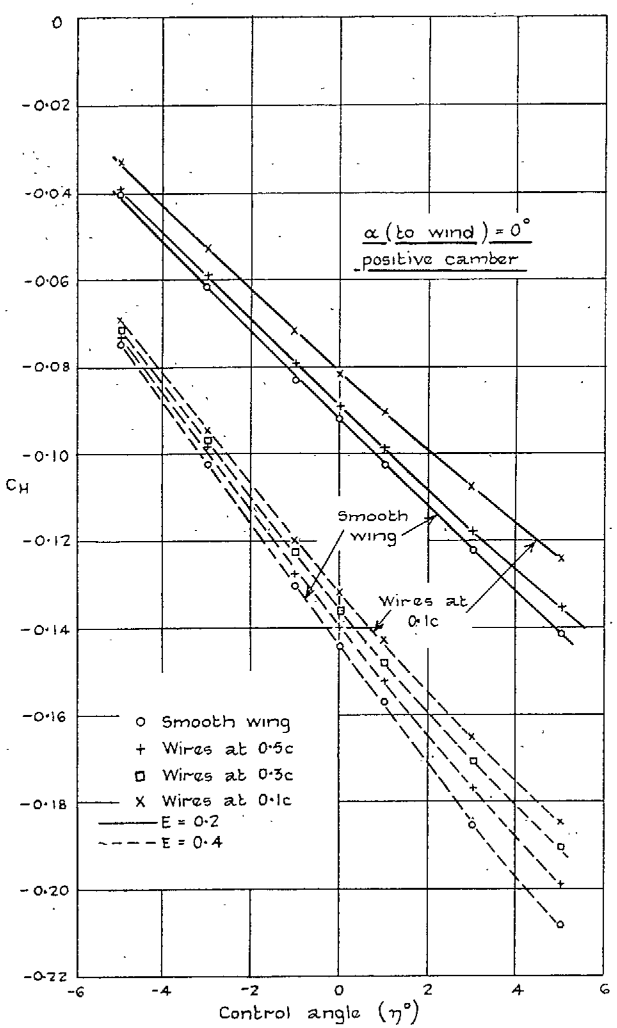

FIG. 8. Uncorrected hinge moment against control setting.

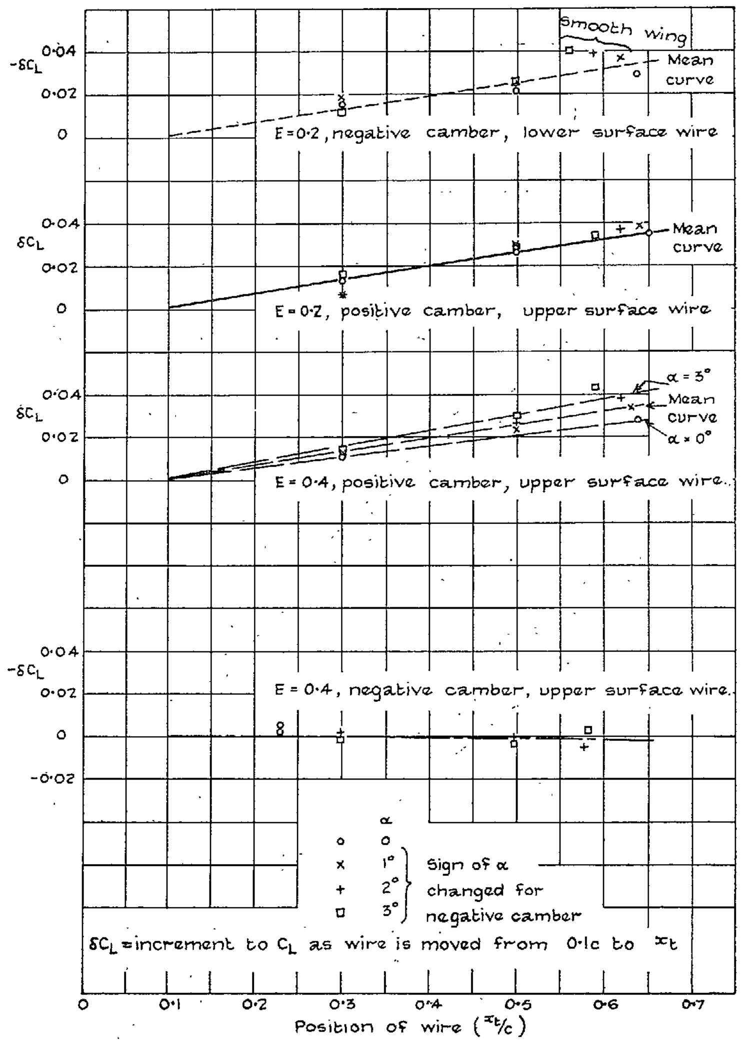

FIG. 9. Variation of lift with transition.

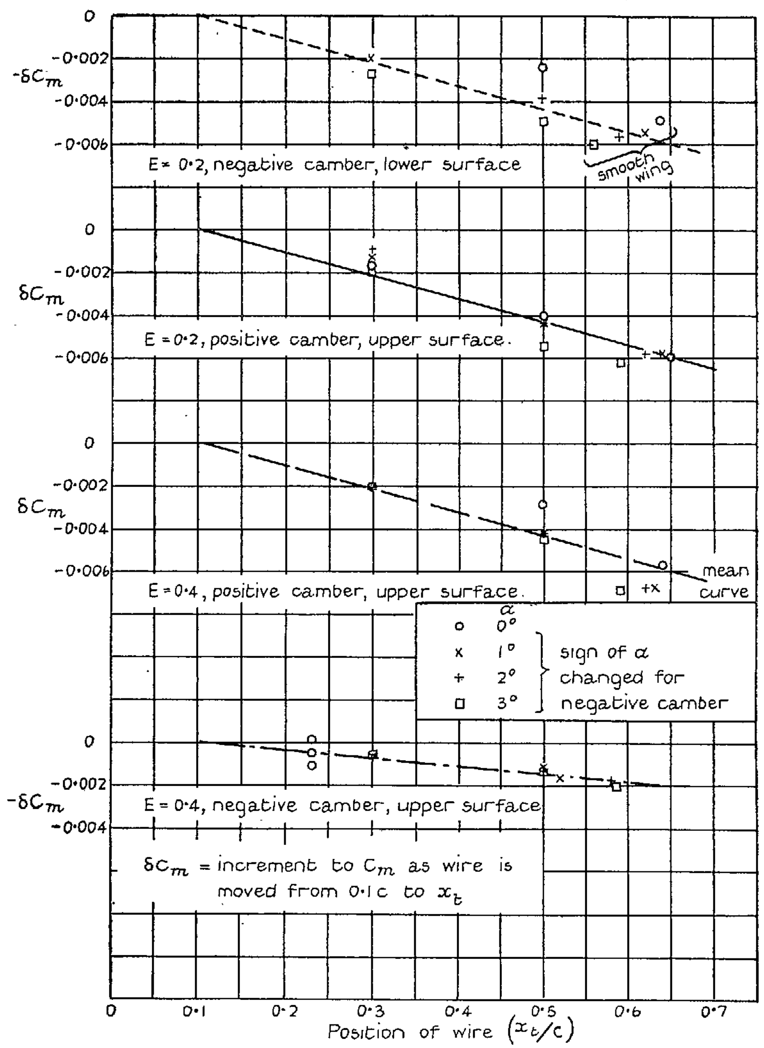

FIG. 10. Variation of pitching moment with transition.

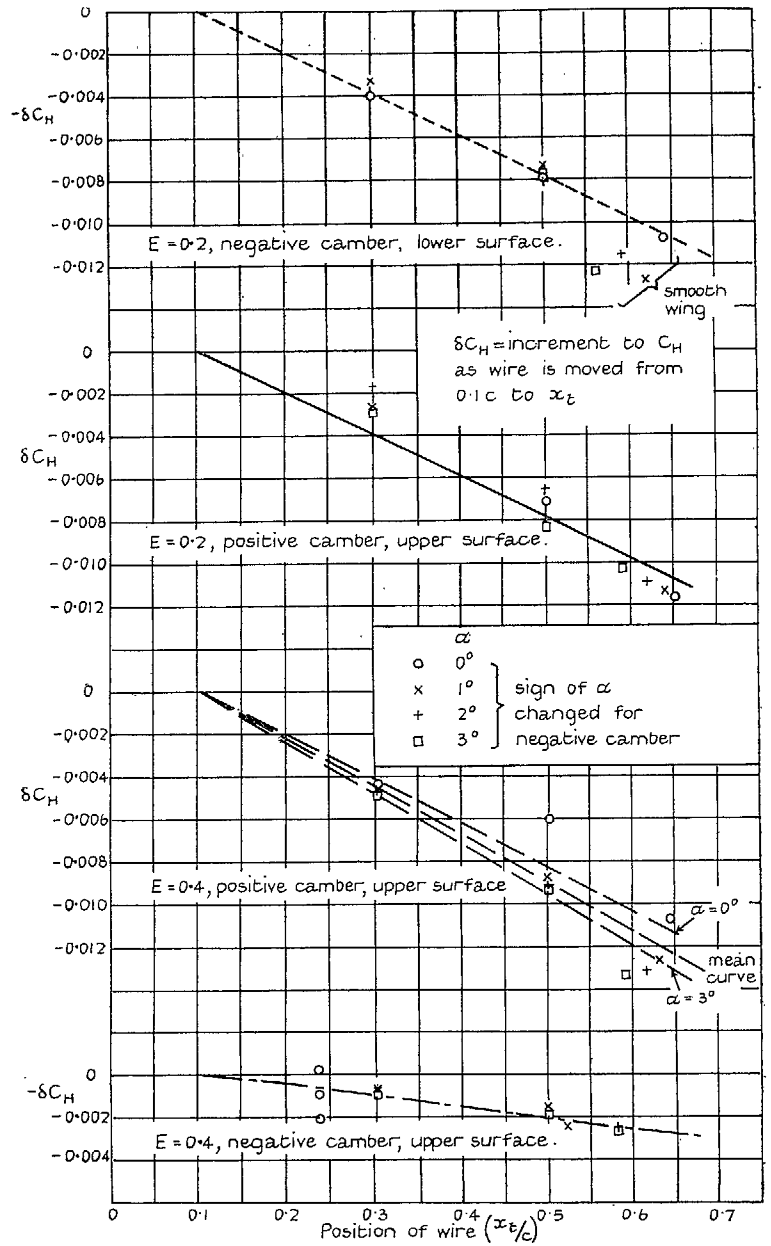

FIG. 11. Variation of hinge moment with transition.

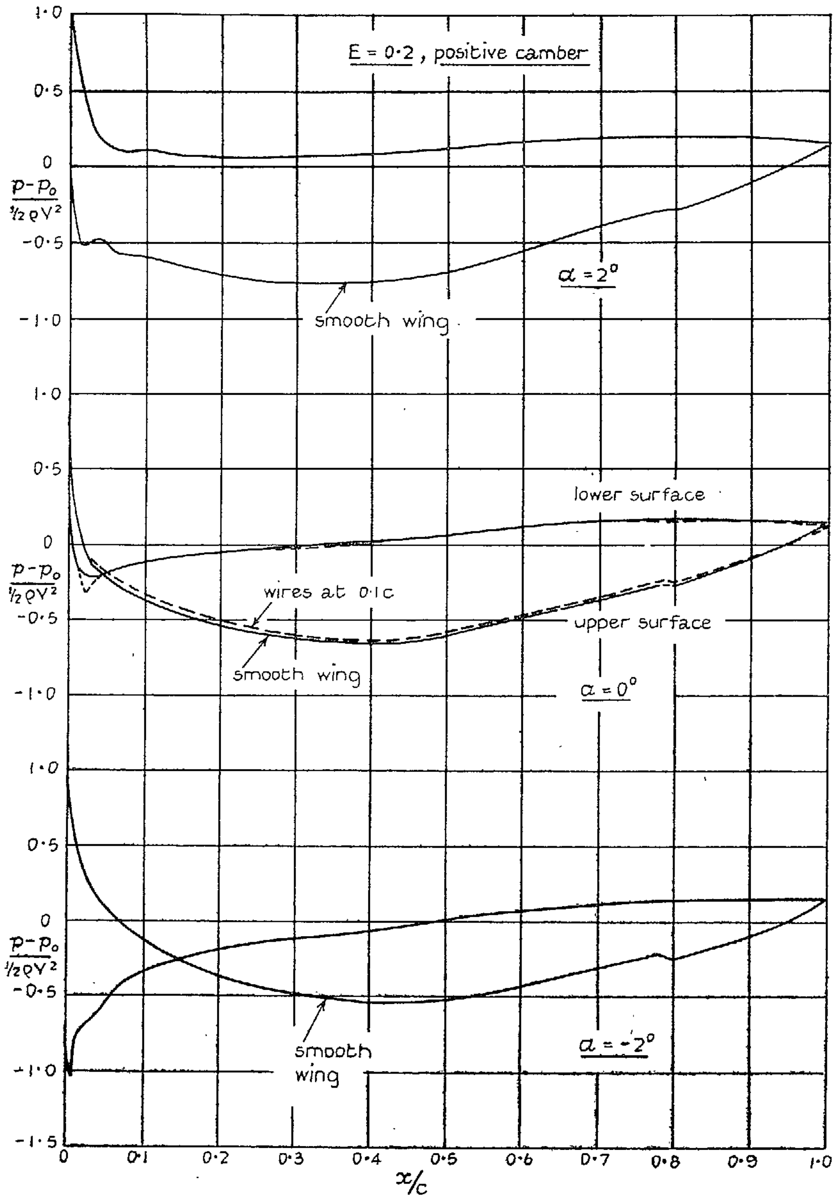

FIG. 12a. Measured pressure distributions at various incidences. α (to wind) = −2, 0 and +2 deg.

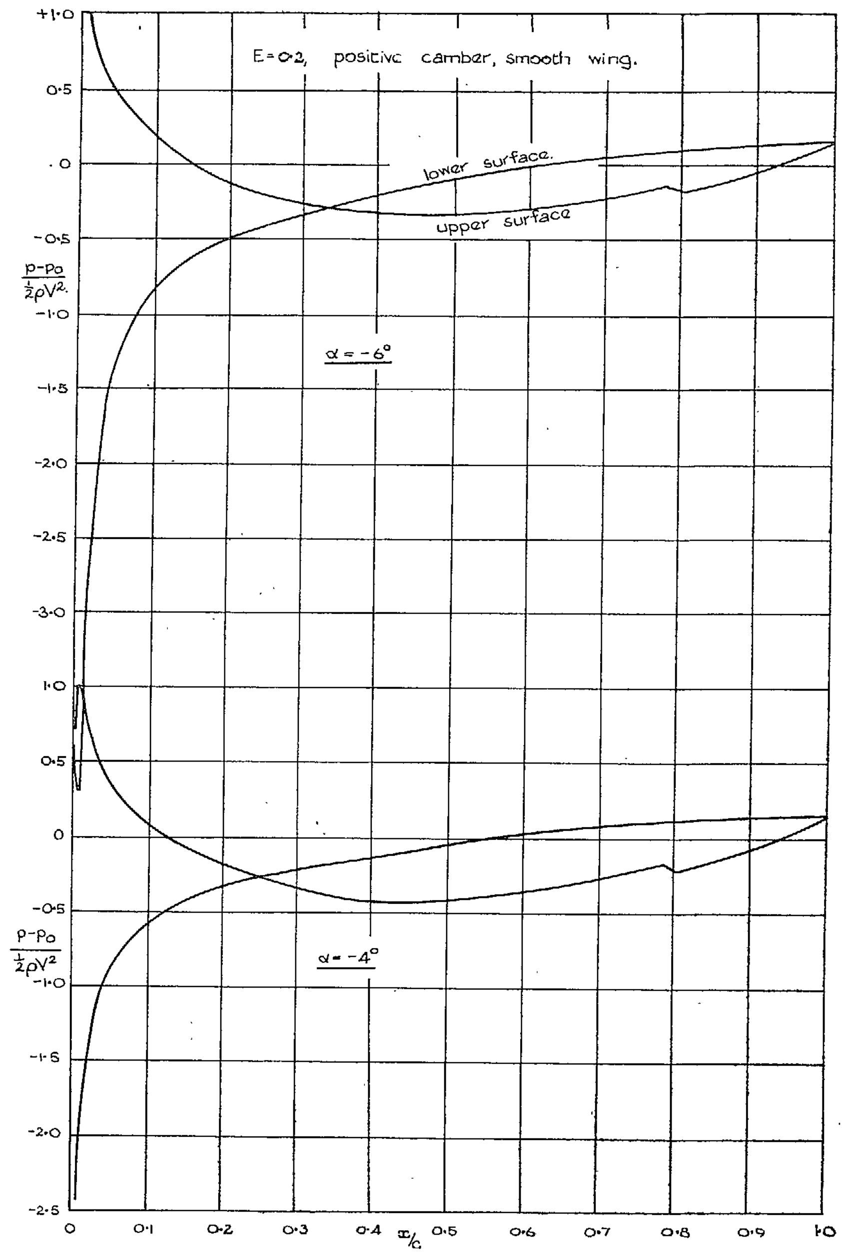

FIG. 12b. Measured pressure distributions at various incidences. α (to wind) = −6 and −4 deg.

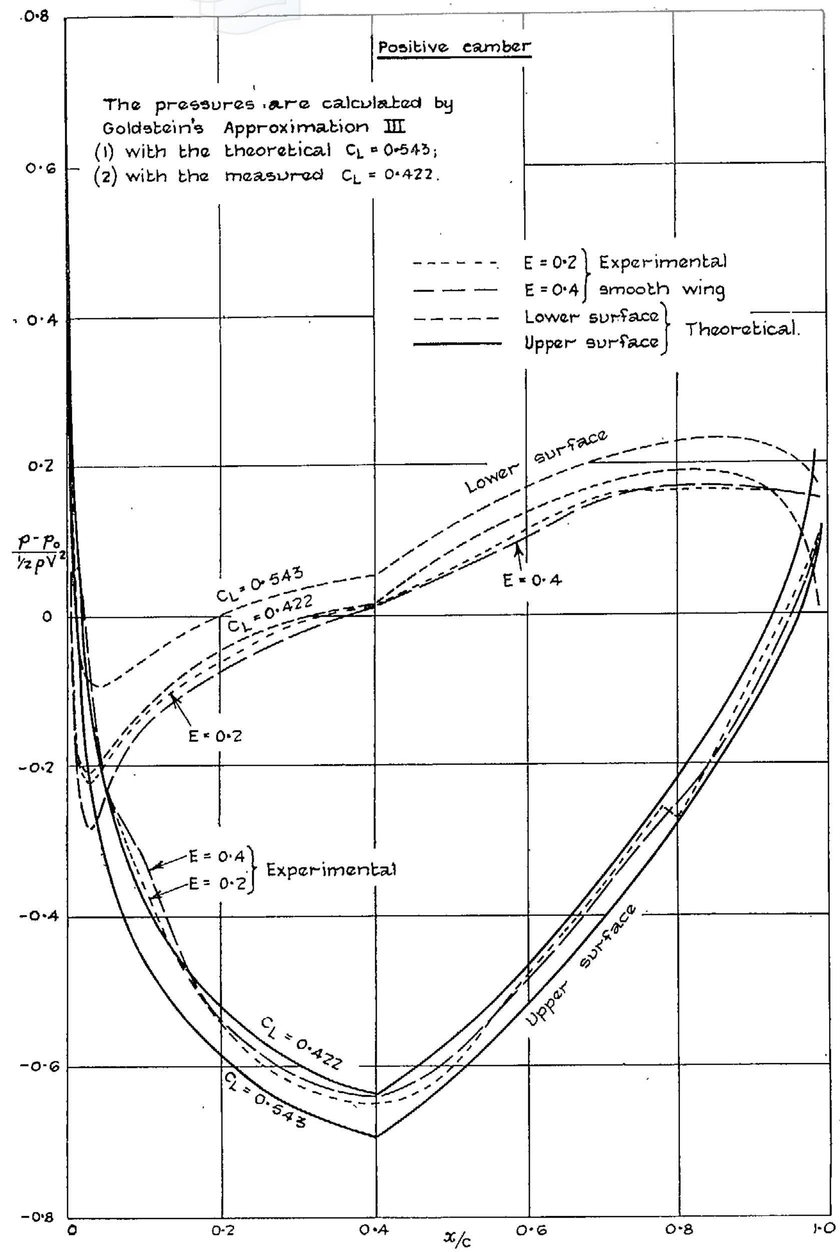

FIG. 13. Measured and theoretical pressure distributions at zero incidence.

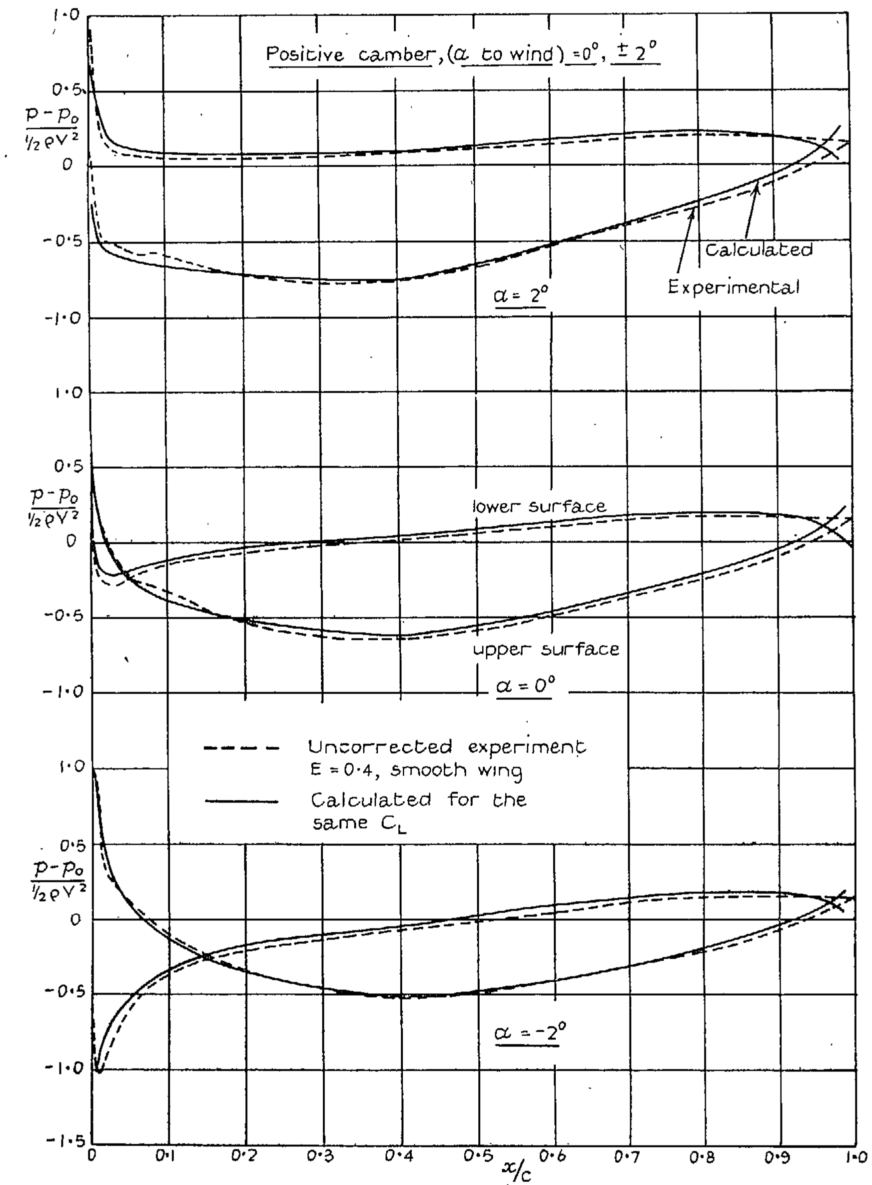

FIG. 14. Measured and calculated pressure distributions.

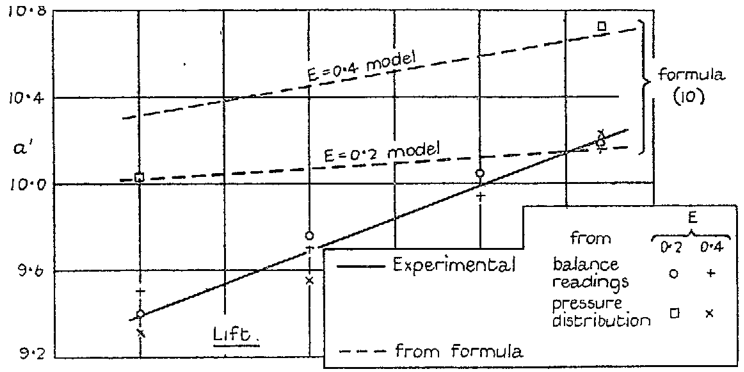

FIG. 15.

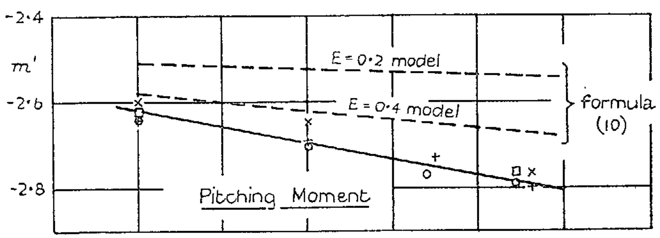

FIG. 16.

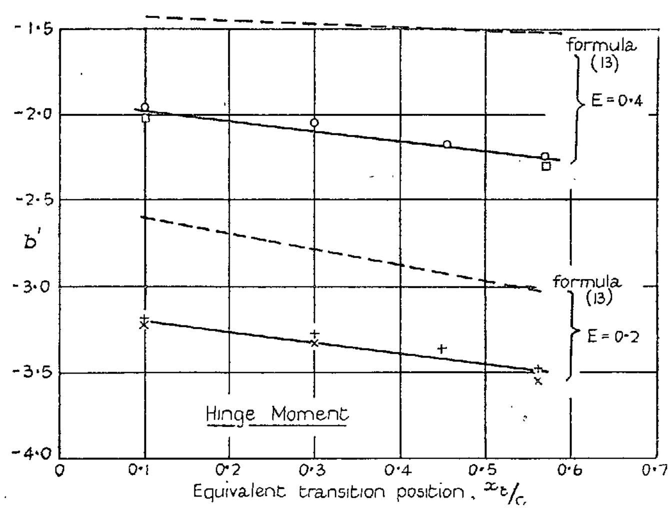

FIG. 17.

FIGS. 15, 16 and 17. Camber derivatives against position of transition.

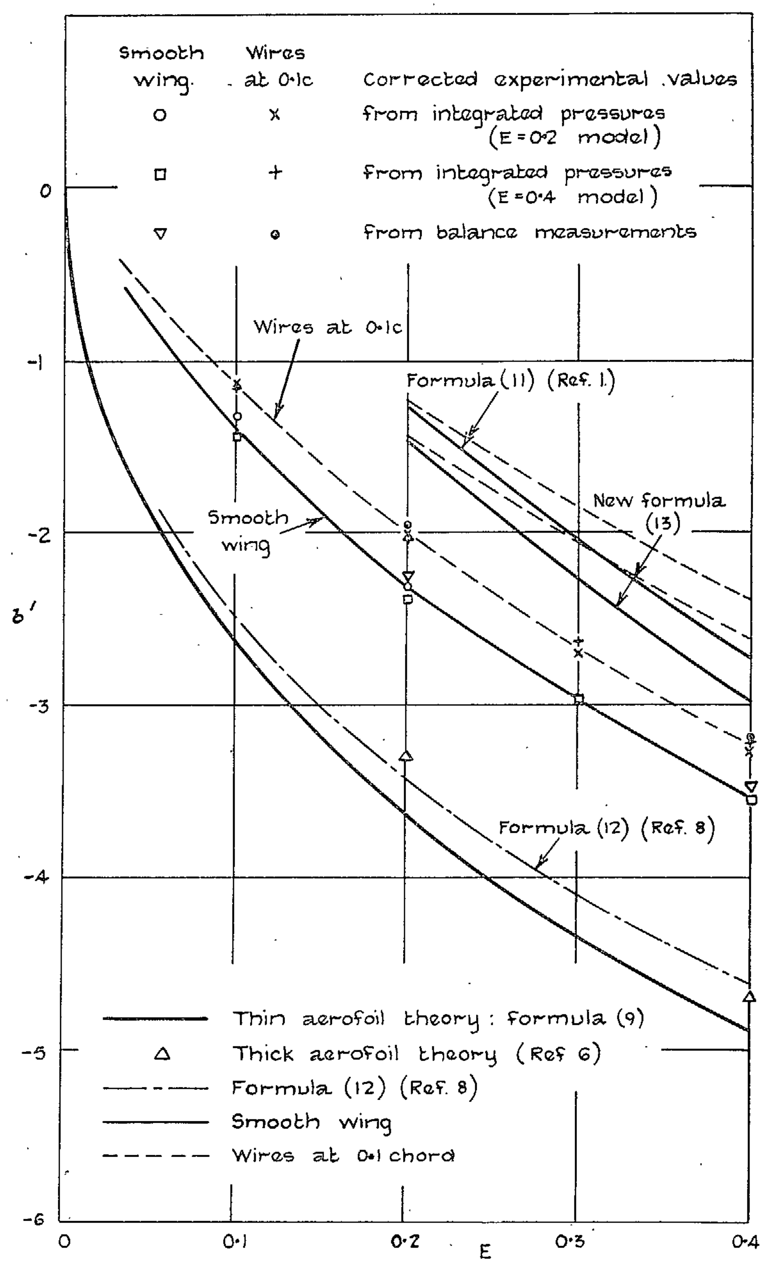

FIG. 18. Variation of b' with control chord.

J4333 Wt.18/9296 K7 10/55 D&Co. 34/263

PRINTED IN GREAT BRITAIN

Publications of the Aeronautical Research Council

ANNUAL TECHNICAL REPORTS OF THE AERONAUTICAL RESEARCH COUNCIL (BOUND VOLUMES)

1938 Vol. I. Aerodynamics General, Performance, Airscrews. 50s. (51s. 2d.)
Vol. II. Stability and Control, Flutter, Structures, Seaplanes, Wind Tunnels, Materials. 30s. (31s. 2d.)

1939 Vol. I. Aerodynamics General, Performance, Airscrews, Engines. 50s. (51s. 2d.)
Vol. II. Stability and Control, Flutter and Vibration, Instruments, Structures, Seaplanes, etc. 63s. (64s. 2d.)

1940 Aero and Hydrodynamics, Aerofoils, Airscrews, Engines, Flutter, Icing, Stability and Control, Structures, and a miscellaneous section. 50s. (51s. 2d.)

1941 Aero and Hydrodynamics, Aerofoils, Airscrews, Engines, Flutter, Stability and Control, Structures. 63s. (64s. 2d.)

1942 Vol. I. Aero and Hydrodynamics, Aerofoils, Airscrews, Engines. 75s. (76s. 3d.)
Vol. II. Noise, Parachutes, Stability and Control, Structures, Vibration, Wind Tunnels. 47s. 6d. (48s. 8d.)

1943 Vol. I. Aerodynamics, Aerofoils, Airscrews. 80s. (81s. 4d.)
Vol. II. Engines, Flutter, Materials, Parachutes, Performance, Stability and Control, Structures. 90s. (91s. 6d.)

1944 Vol. I. Aero and Hydrodynamics, Aerofoils, Aircraft, Airscrews, Controls. 84s. (85s. 8d.)
Vol. II. Flutter and Vibration, Materials, Miscellaneous, Navigation, Parachutes, Performance, Plates and Panels, Stability, Structures, Test Equipment, Wind Tunnels. 84s. (85s. 8d.)

ANNUAL REPORTS OF THE AERONAUTICAL RESEARCH COUNCIL—

1933–34	1s. 6d. (1s. 8d.)	1937	2s. (2s. 2d.)
1934–35	1s. 6d. (1s. 8d.)	1938	1s. 6d. (1s. 8d.)
April 1, 1935 to Dec. 31, 1936	4s. (4s. 4d.)	1939–48	3s. (3s. 2d.)

INDEX TO ALL REPORTS AND MEMORANDA PUBLISHED IN THE ANNUAL TECHNICAL REPORTS, AND SEPARATELY—

April, 1950 - - - - - R. & M. No. 2600. 2s. 6d. (2s. 7½d.)

AUTHOR INDEX TO ALL REPORTS AND MEMORANDA OF THE AERONAUTICAL RESEARCH COUNCIL—

1909–January, 1954 - - - R. & M. No. 2570. 15s. (15s. 4d.)

INDEXES TO THE TECHNICAL REPORTS OF THE AERONAUTICAL RESEARCH COUNCIL—

December 1, 1936 — June 30, 1939.	R. & M. No. 1850.	1s. 3d. (1s. 4½d.)
July 1, 1939 — June 30, 1945. -	R. & M. No. 1950.	1s. (1s. 1½d.)
July 1, 1945 — June 30, 1946. -	R. & M. No. 2050.	1s. (1s. 1½d.)
July 1, 1946 — December 31, 1946.	R. & M. No. 2150.	1s. 3d. (1s. 4½d.)
January 1, 1947 — June 30, 1947. -	R. & M. No. 2250.	1s. 3d. (1s. 4½d.)

PUBLISHED REPORTS AND MEMORANDA OF THE AERONAUTICAL RESEARCH COUNCIL—

Between Nos. 2251–2349. - -	R. & M. No. 2350.	1s. 9d. (1s. 10½d.)
Between Nos. 2351–2449. - -	R. & M. No. 2450.	2s. (2s. 1½d.)
Between Nos. 2451–2549. - -	R. & M. No. 2550.	2s. 6d. (2s. 7½d.)
Between Nos. 2551–2649. - -	R. & M. No. 2650.	2s. 6d. (2s. 7½d.)

Prices in brackets include postage

HER MAJESTY'S STATIONERY OFFICE

York House, Kingsway, London W.C.2; 423 Oxford Street, London W.1 (Post Orders: P.O. Box 569, London S.E.1); 13a Castle Street, Edinburgh 2; 39 King Street, Manchester 2; 2 Edmund Street, Birmingham 3; 109 St. Mary Street, Cardiff; Tower Lane, Bristol 1; 80 Chichester Street, Belfast, *or through any bookseller*

S.O. Code No. 23-2946